Title

Choline Uptake and Metabolism Modulate Macrophage IL-1β and IL-18 Production

Journal

Cell Metabolism, 29(6)

ISSN

1550-4131

Authors

Sanchez-Lopez, Elsa

Zhong, Zhenyu

Stubelius, Alexandra

et al.

Publication Date

2019-06-01

DOI

10.1016/j.cmet.2019.03.011

Peer reviewed

Published in final edited form as:

Cell Metab. 2019 June 04; 29(6): 1350–1362.e7. doi:10.1016/j.cmet.2019.03.011.

Choline uptake and metabolism modulate macrophage IL-1β and IL-18 production

Elsa Sanchez-Lopez[1], **Zhenyu Zhong**[1,5], **Alexandra Stubelius**[2], **Shannon R. Sweeney**[7], **Laela M. Booshehri**[4], **Laura Antonucci**[1], **Ru Liu-Bryan**[2,3], **Alessia Lodi**[6,7], **Robert Terkeltaub**[2,3], **Juan Carlos Lacal**[9], **Anne N. Murphy**[1], **Hal M. Hoffman**[4], **Stefano Tiziani**[6,7,8], **Monica Guma**[2], **Michael Karin**[1,*]

[1]Departments of Pharmacology and Pathology, University of California San Diego, La Jolla, CA, 92037, USA

[2]Division of Rheumatology, Allergy and Immunology, University of California San Diego, La Jolla, CA, 92037, USA

[3]VA San Diego Healthcare System, University of California San Diego, La Jolla, CA, 92037, USA

[4]Department of Pediatrics and Rady Children's Hospital, University of California San Diego, La Jolla, CA, 92037, USA

[5]Department of Immunology, University of Texas Southwestern Medical Center, 6000 Harry Hines Blvd, Dallas TX 75390, USA

[6]Department of Molecular Biosciences, College of Natural Sciences; The University of Texas at Austin, Austin, TX, 78723-3092, USA

[7]Department of Nutritional Sciences, The University of Texas at Austin, Austin, TX, 78723-3092, USA

[8]Department of Pediatrics, Dell Medical School, The University of Texas at Austin, Austin, TX, 78723-3092, USA

[9]Translational Oncology. Department of Oncology. Hospital Universitario Fuenlabrada, Instituto de Investigación Sanitaria IdiPAZ, Madrid, Spain

[*]Lead Contact.

SUMMARY

Choline is a vitamin-like nutrient that is taken up via specific transporters and metabolized by choline kinase which converts it to phosphocholine needed for *de novo* synthesis of

Correspondence: karinoffice@ucsd.edu.

AUTHOR CONTRIBUTIONS

E.S-L. conceived the project, designed and performed most of the experiments. Z.Z. and L.A. provided assistance with experiments and analyses. A.S. and M.G. performed and analyzed air pouch model. R.L-B. provided *AMPKα1*$^{-/-}$ mice. S.R.S., A.L. and S.T. performed NMR and MS analysis. H.M.H. and L.M.B. provided *Nlrp3* mutant mice and performed MWS mouse model and *in vitro* experiments. J.C.L. provided ChoKα inhibitors. Z.Z., R.T., R.L-B., J.C.L., A.N.M., H.M.H., M.G. and M.K. provided advice. M.K. supervised the project. E.S-L. and M.K. wrote the manuscript with input from all authors.

DECLARATION OF INTERESTS

The University of California San Diego is in the process of applying for a patent covering the use of CTL1 and/or Choline kinase genetic/chemical inhibitors to treat NLRP3 inflammasome-associated diseases listing E.S-L. and M.K. as inventors.

phosphatidylcholine (PC), the main phospholipid of cellular membranes. We found that Tolllike receptor (TLR) activation enhances choline uptake by macrophages and microglia through induction of the choline transporter CTL1. Inhibition of CTL1 expression or choline phosphorylation attenuated NLRP3 inflammasome activation and IL-1β and IL-18 production in stimulated macrophages. Mechanistically, reduced choline uptake altered mitochondrial lipid profile, attenuated mitochondrial ATP synthesis and activated the energy sensor AMP-activated protein kinase (AMPK). By potentiating mitochondrial recruitment of DRP1, AMPK stimulates mitophagy, which contributes to termination of NLRP3 inflammasome activation. Correspondingly, choline kinase inhibitors ameliorated acute and chronic models of IL-1β-dependent inflammation.

INTRODUCTION

Macrophages respond to pathogens and tissue damage via pattern recognition receptors (PRR) that sense pathogen (PAMP) or damage (DAMP) associated molecular patterns (Martinon et al., 2009). NLRP3, a member of the Nod-like receptor (NLR) family that is induced on macrophage activation, senses cytosolic oxidized mitochondrial DNA (ox-mtDNA) that is generated when activated macrophages are exposed to NLRP3-activating DAMPs, such as ATP or uric acid, and triggers IL-1β and IL-18 production and secretion (Zhong et al., 2018). While NLRP3 serves as its specific sensor subunit, the NLRP3 inflammasome also consists of the adaptor apoptosis-associated speck-like protein containing CARD (ASC), and the effector enzyme pro-caspase-1, which undergoes autocleavage upon inflammasome activation, and is responsible for production of IL-1β and IL-18 (Elliott and Sutterwala, 2015; Martinon et al., 2009). Given the involvement of the NLRP3 inflammasome and IL-1β in many diseases, including type 2 diabetes, atherosclerosis, gout, rheumatoid arthritis, non-alcoholic steatohepatitis (NASH), lupus, and Alzheimer's disease (Busso and So, 2010; Heneka et al., 2013; Zhong et al., 2016b), it is not surprising that both initiation and termination of NLRP3 inflammasome activation are intricately regulated (Zhong et al., 2016a).

Choline is an essential human nutrient, serving as precursor for membrane phospholipids, acetylcholine, and functioning as a methyl group donor when metabolized to betaine and subsequently to S-adenosylmethionine (Aoyama et al., 2004). Choline uptake is mediated by choline transporters, of which choline-transporter-like proteins (CTL) 1–5 are preferentially used to provide choline to Choline Kinase alpha (ChoKα), the first enzyme in phosphatidylcholine synthesis (Traiffort et al., 2005). Increased circulating choline and its enhanced uptake were observed in inflammatory diseases, including arthritis, cardiovascular diseases, and cancer (Al-Saffar et al., 2006; Guma et al., 2015a; Hellberg et al., 2016; Seki et al., 2017). The use of choline as a tracer for enhanced cancer cell proliferation was established a few decades ago. More recently, the observation that activated cells, including fibroblasts and macrophages, take up choline at inflammatory sites suggested that choline may also have other biological functions. Here we show that choline uptake via CTL1 and its phosphorylation by ChoKα contribute to macrophage-mediated IL-1β-dependent inflammation. Impaired choline uptake or phosphocholine production affect mitochondrial phosphatidylcholine and sphingomyelin, disrupt mitochondrial ATP synthesis and trigger

AMPK activation and mitophagy. By decreasing the number of damaged mitochondria that produce oxidized (ox)-mtDNA, the ultimate NLRP3 activator, mitophagy attenuates IL-1β production. Correspondingly, inhibition of phosphocholine synthesis ameliorates acute and chronic NLRP3-dependent inflammation.

RESULTS

LPS induces macrophage CTL1/Slc44a1 and choline uptake

Exposure of bone-marrow-derived macrophages (BMDM) to LPS increased *Slc44a1* mRNA (Figure 1A), coding for the choline transporter CTL1 (Figures 1B and 1C). CTL1 induction correlated with enhanced choline uptake (Figure 1D). LPS also induced rapid choline mobilization via the Kennedy pathway, increasing cellular phosphocholine, glycerol-3-phosphocholine and phosphatidylcholine (PC) content, an effect that was blocked by the ChoKα inhibitor RSM932A (Figures S1A, S1B and S1C). In microglia, the myeloid cells of the central nervous system, LPS induced Slc44a1/CTL1 as well as *ChKa* mRNA (Figure S1D). Thus, enhanced choline uptake and phosphorylation is a general response to LPS stimulation of myeloid cells.

LPS rapidly activates NF-KB-dependent transcription to produce inflammatory mediators and cytokines (Ben-Neriah and Karin, 2011; Greten et al., 2007). NF-kB inhibition by IKKp ablation or the IKKp inhibitor BMS345541 blocked Slc44a1/CTL1 induction (Figures 1E and S1E).

Impaired choline uptake reduces NLRP3 inflammasome activation

NF-kB activation also induces expression of pro-IL-1β and NLRP3, as well as numerous cytokines and chemokines (Vallabhapurapu and Karin, 2009). We examined the impact of *Slc44a1* gene knockdown on LPS-induced responses. *Slc44a1* gene knockdown did not affect other choline-related mRNAs (Figure 2A). Importantly, *Slc44a1* knockdown reduced IL-1β and IL-18 production in response to different NLRP3 inflammasome activators, including ATP, nigericin, and monosodium urate (MSU) microcrystals (Figures 2B and S2A). *Slc44a1* knockdown also decreased TNF production but had no effect on IL-6 release (Figures S2B and S2C). Reduced IL-1β production on *Slc44a1* knockdown correlated with diminished caspase-1 activation (Figure 2C and 2D). Culturing of BMDM in choline-deficient medium (so-called choline-free medium), also interfered with IL-1β (Figure 2E) and IL-18 production (Figure S2D), and caspase-1 activation (Figures 2F and 2G), but had no effect on AIM2 inflammasome-mediated IL-1β production (Figure S2E). Culture in choline-free medium, however had no effect on TNF and IL-6 production (Figures S2F and S2G). Choline deficiency did not cause intracellular accumulation of mature IL-1β, ruling out an effect on the secretory system responsible for IL-1β release (Figure 2H).

Slc44a1 ablation had no significant effect on synthesis of *Il1b* or *Tnf* mRNAs (Figures S2H and S2I). The LPS-induced anti-inflammatory cytokine IL-10 restrains IL-1β production by limiting glucose uptake and the glycolytic switch through autocrine induction of the mTORC1 inhibitor DDIT4 (Ip et al., 2017). *Slc44a1* ablation did not affect *Il10* mRNA expression (Figure S2J), and choline deficiency reduced IL-1β production in *Il10rb*$^{-/-}$

BMDM (Figure S2K). *Il10rb*$^{-/-}$BMDM exhibited normal upregulation of *Slc44a1* after LPS stimulation (Figure S2L), suggesting that the mechanisms by which IL-10 and choline deficiency control IL-1β production are different.

Nitric oxide (NO) limits IL-1β production independent of its antimicrobial function (Mishra et al., 2013). shSlc44a1 iBMDM showed similar nitrite secretion (Figure S2M) and *Nos2* mRNA expression (Figure S2N) to shCtrl iBMDM, suggesting that NO is not involved in reduced IL-1β production after choline uptake impairment.

NRLP3 inflammasome activation involves influx of calcium into the cytosol (Lee et al., 2012; Murakami et al., 2012; Zhong et al., 2013) and efflux of potassium (Munoz-Planillo et al., 2013). Choline deficiency did not affect calcium (Figure S2O) or potassium (Figure S2P) fluxes. Collectively, these results indicate that choline uptake regulates activation of the NLRP3 inflammasome and caspase-1. However, choline uptake via CTL1 does not affect the IL-10-dependent glycolytic switch or changes in intracellular calcium and potassium.

Choline phosphorylation contributes to IL-1β production

After LPS stimulation, choline is taken up and rapidly converted to phosphocholine by ChoKα (Figure S1A). ChoKα knockdown reduced IL-1β production (Figure 3A). Pretreatment with the ChoKα inhibitor RSM932A (Lacal and Campos, 2015) produced a similar effect (Figure 3B). Furthermore, ChoKα knockdown (Figures 3C and 3D) and RSM932A treatment (Figures 3E and 3F) inhibited caspase-1 activation. Inhibition or knockdown of ChoKα did not alter expression of NLRP3 inflammasome components, including caspase-1, NLRP3, ASC, or the amount of pro-IL-1β induced by LPS (Figure 3G and 3H).

LPS alters mitochondrial phospholipid and sphingolipid profile

LPS stimulation of BMDM altered mitochondrial lipid profile, decreasing PC and phosphatidylglycerol (PG) content, and increasing phosphatidylserine (PS) and sphingomyelin (SM) content (Figure 4A). LPS, however, did not alter mitochondrial phosphatidylethanolamine (PE) or phosphatidylinositol (PI). Choline deficiency also reduced mitochondrial PC (mitoPC) and increased mitochondrial SM (mitoSM), (Figure S3A), changes that were more pronounced after LPS stimulation (Figures 4B and 4C). Interruption of *de novo* PC synthesis with the ChoKα inhibitor RSM932A showed similar results in mitoPC and mitoSM (Figures S3B and S3C).

Choline deficiency activates AMPK to inhibit IL-1β production

IL-1β production is tightly regulated by metabolic changes. LPS potentiates glycolysis and shuts down oxidative phosphorylation, which results in lower NAD^+/NADH ratio and intracellular ATP (Mills and O'Neill, 2016). Of note, phosphocholine preserves mitochondrial activity by facilitating removal of uncoupling free fatty acids and converting them to phospholipids (Rossi et al., 1962). In addition, altered mitochondrial membrane integrity due to distorted lipid content affects mitochondrial function and biogenesis (Guo et al., 2005; James et al., 1992; Teodoro et al., 2008). LPS stimulation reduced the NAD^+/NADH ratio, indicating diminished complex I forward activity, regardless of choline status

(Figure 4D). Complex V activity and intracellular ATP were reduced in the absence of choline (Figures 4E and 4F). Knockdown of Slc44a1 or ChoKα also reduced intracellular ATP after LPS stimulation (Figures S3D and S3E) without affecting the NAD^+/NADH ratio (Figure S3F), indicating a role of phosphocholine in preserving mitochondrial function. Low intracellular ATP results in AMPK activation which suppresses production of inflammatory cytokines, including IL-1β, through a poorly defined mechanism (O'Neill and Hardie, 2013; Steinberg and Kemp, 2009; Wang et al., 2016). Choline deficiency caused AMPK activation even after LPS stimulation (Figure 4G and 4H). Slc44a1 or ChoKα knockdown and ChoKα pharmacological inhibition also promoted AMPK activation (Figures S3G-S3L). AMPK activation by the selective AMPK agonist A769662 significantly reduced IL-1β production (Figure S3M). Consistently, BMDM lacking AMPKα1, the predominant catalytic subunit, showed enhanced IL-1β release, and choline deficiency in these cells no longer reduced IL-1β production (Figure 4I). Consistent with inhibition of ATP synthase activity, choline deficiency induced accumulation of ATP synthase inhibitory factor 1 (ATPIF1) (Figures 4G and 4J). After LPS stimulation, and together with reduction of oxidative phosphorylation, the TCA cycle is also impacted. LPS induces accumulation of two TCA cycle intermediates, citrate and succinate (Tannahill et al., 2013), that potentiate production of NO and PGE2, and IL-1β respectively. However, culture in choline-free medium had no effect on LPS-induced succinate accumulation (Figure S3N).

Impaired choline uptake and phosphorylation stimulate mitophagy

AMPK activation stimulates autophagy/mitophagy via phosphorylation of ULK1 and mitochondrial fission factor (MFF), a mitochondrial outer-membrane receptor for DRP1 (Egan et al., 2011; Toyama et al., 2016). DRP1 binds to fission sites, which isolate mitochondria with reduced membrane potential, thereby enhancing recruitment of the mitophagy-promoting E3 ubiquitin ligase Parkin (Narendra et al., 2008). We have recently shown that NF-KB-induced mitophagy facilitates removal of damaged mitochondria, which produce the NLRP3-activating ligand ox-mtDNA (Zhong et al., 2018; Zhong et al., 2016c). Knockdown of ChoKα or its pharmacological inhibition with RSM932A reduced mitochondrial membrane potential (Ψm), at least as effectively as the uncoupler carbonyl cyanide m-chlorophenyl hydrazone (CCCP) (Figures 5A and 5B). Loss of Ψm enhanced mitochondrial recruitment of the autophagy adaptor p62/Sqstm1 (Figures 5C and 5D) and DRP1 (Figures 5E, 5F and S4A–C), indicating that lack of functional ChoKα activates mitophagy. Choline deficiency also potentiated p62 and DRP1 mitochondrial recruitment (Figures S4D-F). Importantly, AMPKa1 KO BMDM exhibited increased p62 recruitment to the mitochondria regardless of choline availability (Figures 5G and 5H), however DRP1 was mainly located in the cytosol, indicating impaired mitophagy (Figure 5I). Consistently, inhibition of mitophagy through *Atg7* knockdown enhanced IL-1β production and abrogated its downregulation in response to reduced choline uptake (Figure S4G). Consistent with mitophagic elimination of damaged mitochondria, ChoKα knockdown and inhibition attenuated production of mitochondrial reactive oxygen species (mtROS) in macrophages stimulated with NLRP3 inflammasome activators (Figures S4H and S4I). Furthermore, ChoKα knockdown or inhibition reduced release of fragmented mtDNA to the cytosol (Figure S4J and S4K).

ChoKα inhibition reduces IL-1β-dependent acute inflammation

To validate our *in vitro* results under more physiologically relevant conditions, we used two different acute experimental models that are NLRP3-inflammasome-dependent. First, mice were subjected to LPS-induced septic shock. ChoKα was inhibited by MN58b treatment daily for 3 days prior to LPS challenge. Importantly, ChoKα inhibition prevented LPS-induced death (Figure 6A), and this was associated with reduced circulating IL-1β (Figure 6B). As found *in vitro,* ChoKα inhibition did not inhibit TNF or IL-6 production (Figures S5A and S5B). We also used synovium-like gout air-pouch model. Once the air pouch was created, mice were pretreated with MN58b 24 hr before injection with MSU crystals into the pouch to elicit NLRP3 inflammasome activation and acute gouty inflammation (Hoffman et al., 2010; Martinon et al., 2006; Wang et al., 2016). MSU crystal challenge caused recruitment of macrophages that expressed CTL1 and ChoKα into the pouch (Figure 6C). Pretreatment with the ChoKα inhibitor attenuated total leukocyte recruitment into the pouch and reduced production of IL-1β (Figures 6D and 6E). Together these results indicate that choline phosphorylation is important for mounting acute inflammatory responses and that ChoKα inhibition can attenuate inflammation *in vivo.*

ChoKα inhibition reduces Muckle-Wells syndrome severity

Cryopyrin-associated periodic syndromes (CAPS) include three genetic diseases, Muckle-Wells syndrome (MWS), familial cold autoinflammatory syndrome (FCAS) and neonatal onset multisystem inflammatory disease (NOMID), that arise from *NLRP3* gene mutations that cause inflammasome activation (Hoffman et al., 2001). IL-1β production in BMDM isolated from MWS $Nlrp3^{A350VneoRCreT}$, FCAS $Nlrp3^{L351PneoCreT}$, and NOMID $Nlrp3^{D301NneoCreT}$ conditional knock-in mice, was decreased in the absence of choline or in the presence of ChoKα inhibitor (Figures 7A, 7B and 7C). Of note, treatment with MN58b attenuated MWS pathogenesis *in vivo*, as shown by reduction in total white blood cells count (Figure 7D), including granulocytes (Figure 7E) and monocytes (Figure 7F), without an effect on lymphocyte counts (Figure 7G). In addition, MN58b reduced MWS splenomegaly (Figures 7H and 7I), and liver size, most likely due to reduced immune cell infiltration (Figures 7J and 7K).

DISCUSSION

Enhanced choline uptake was detected in cells within inflammatory sites, including tumors, inflamed joints, and atherosclerotic plaques (Hellberg et al., 2016; Matter et al., 2006; Roivainen et al., 2003; Schwarz et al., 2016). However, the biological impact of choline uptake and phosphorylation has only been studied in cancer, where choline feeds the phospholipid pool required for cell proliferation and migratory/invasive behavior (Al-Saffar et al., 2006; Glunde et al., 2011). Tracer studies demonstrated that under pathological inflammatory conditions choline is taken up by macrophages (Hellberg et al., 2016; Matter et al., 2006; Roivainen et al., 2003; Schwarz et al., 2016), but the effect of choline uptake on macrophage biology was heretofore unknown. Now we show that TLR4-mediated macrophage activation results in upregulation of choline uptake due to NF-KB-dependent induction of the choline transporter CTL1. The newly taken up choline is rapidly converted to PC via the Kennedy pathway. Inhibition of CTL1 expression or ChoKα-mediated choline

mobilization results in altered mitochondrial phospholipid composition and accumulation of defective mitochondria, that are rapidly eliminated through mitophagy. These results strongly suggest that choline uptake is essential for phospholipid remodeling and maintenance of mitochondrial function and integrity in metabolically challenged/stressed macrophages.

Macrophage activation involves extensive metabolic reprogramming, a glycolytic switch, elevated ROS production, and phospholipid remodeling that are needed for coping with the energetic cost of inflammatory cytokine production and bactericidal activity, and to ensure proper membrane fluidity and plasticity (Chu, 1992; Grove et al., 1990; Tian et al., 2008). Ablation of macrophage choline cytidylyltransferase a (CCTα), which uses phosphocholine to generate CDP-choline, in the second step of the Kennedy pathway reduces cellular PC amounts with a subsequent decrease in accumulation of diacylglycerol (DAG), which interferes with TNF secretion (Tian et al., 2008). Contrary to TNF and IL-6, bioactive IL-1β is not secreted via the classical secretory pathway. IL-1β and IL-18 production and release require macrophage priming, during which pro-IL-1β, pro-IL18 and the critical inflammasome sensor NLRP3 are made. Next, a variety of secondary stimuli, such as ATP, MSU crystals, microbial toxins, and various microcrystals and microfibers, all of which cause mitochondrial damage (Zhou et al., 2011), ROS production (West et al., 2011) and the release of ox-mtDNA fragments (Zhong et al., 2018), trigger NRLP3 inflammasome assembly and activation. This results in conversion of pro-IL-1β and pro-IL18 to their mature forms, which are released from activated macrophages by non-traditional protein secretion. Defective choline uptake or inhibition of phosphocholine synthesis interfere with IL-1β and IL-18 production by accelerating mitophagy and diminishing the cytosolic release of the ultimate N LRP3 inflammasome activator ox-mtDNA. Since sustained NLRP3 inflammasome activation and IL-1β production require some form of mitochondrial damage, ongoing mtROS production, and new mtDNA synthesis (Zhong et al., 2018), it appears that proper PC synthesis is needed for maintaining mitochondrial membrane integrity after LPS priming, thereby preventing excessive damage that could result in defective ATP production and upregulation of AMPK-dependent mitophagy.

The effect of choline deficiency was studied in liver. Mice fed a choline-deficient diet shows alterations in hepatocyte mitochondrial membrane composition, and undergo depletion of PC and PE (Guo et al., 2005; Teodoro et al., 2008). These changes cause loss of mitochondrial membrane potential and reduced activity of the electron transport chain complex I and V (Guo et al., 2005; James et al., 1992). In choline-deficient macrophages, mitoPC and mitoSM are significantly reduced, mitochondrial membrane potential drops and ATP synthase, a part of complex V, activity declines. Of note, LPS also altered mitoPC and mitoSM and reduced ATP synthase activity, events that were strongly modified by choline deficiency. Choline taken up after LPS stimulation may maintain mitochondrial integrity and function, thereby preserving residual ATP synthase activity needed for IL-1β production, a suggestion that is consistent with previous observations (Mills et al., 2016). The reduction in ATP synthase activity caused by choline deficiency is accompanied by accumulation of ATPIF1, a protein that not only inhibits the forward ATP synthase activity of complex V but also blocks the reverse reaction, in which ATP is hydrolyzed (Campanella et al., 2009). This protective response prevents excessive ATP expenditure during times of reduced

mitochondrial ATP synthesis, and attenuates ROS production caused by ATP hydrolysis and reverse electron transport (Campanella et al., 2009). Consistently, ChoK knockdown or inhibition by RSM932A, attenuate mtROS production in activated macrophages, and in human cancer cells using an unrelated ChoK inhibitor (Trousil et al., 2016). Although we do not know exactly how choline deficiency and reduced mitoPC and mitoSM content affect mitochondrial function, it is plausible that changes in mitochondrial membrane composition interfere with complex V assembly or function without increasing mtROS production. It is also possible that intracellular choline or phosphocholine are sensed by a mitochondrial protein, which induces protective responses that prevent mitochondrial failure during reduced phosphocholine availability. Alternatively, insufficient cellular PC interferes with ongoing membrane synthesis needed for maintenance of mitochondrial integrity. A regulatory role for membrane lipid composition in activated macrophages was also proposed by others. Phosphatidylinositol-4-phosphate in the trans-Golgi network (Chen and Chen, 2018), and cholesterol uptake and distribution in ER membranes (de la Roche et al., 2018) also contribute to NLRP3 inflammasome activation. Reduced mitochondrial ATP production results in low cellular ATP, elevated AMP/ATP ratio and activation of AMPK, which stimulates initiation of autophagy and accelerates mitophagic clearance of defective mitochondria. LPS stimulation rapidly represses AMPK activation, but the effect is transient and at later time points AMPK is activated in part via LPS-induced IL-10 to balance the energy and metabolic demands of activated macrophages (Ip et al., 2017; Nomura et al., 2015). Active AMPK downregulates inflammation, in part through inhibition of IL-1β production (Cordero et al., 2018; Guma et al., 2015b; Wang et al., 2016). In addition, we have shown, mitophagy removes damaged mitochondria that release ox-mtDNA, needed for NLRP3 inflammasome activation (Zhong et al., 2018; Zhong et al., 2016c). AMPK stimulates mitophagy both through phosphorylation and activation of ULK1 (Egan et al., 2011), and by enhancing translocation of DRP1 to mitochondria (Toyama et al., 2016). Indeed, in the absence of AMPK, choline deprivation has no effect whatsoever on IL-1β production and secretion, due to DRP1 sequestration in the cytosol leading to defective mitophagy.

Prophylaxis with antibiotics is used to prevent septicemia, however, 40 to 50% of microorganisms at infection sites are antibiotic resistant (Li and Webster, 2018). Notably, prophylactic treatment with ChoK inhibitor protects mice from lethal septic shock. ChoK inhibition reduces IL-1β production and inflammation in LPS-induced septic shock and airpouch gouty arthritis models, showing that choline uptake and phosphorylation are important *in vivo*. Furthermore, ChoKα inhibition reduces IL-1β production and ameliorates MWS, a genetic disease caused by constitutive NLRP3 inflammasome activation, which so far can only be treated with IL-1 sequestering antibodies and decoy receptors. These results further indicate that ChoKα inhibitors may be useful for reducing IL-1β production in other diseases associated with excessive NLRP3 inflammasome activation, such as osteoarthritis, gout, diabetes and Alzheimer's disease. Recently, it was found that in addition to decreasing the incidence of recurrent vascular events in atherosclerotic patients, treatment with an IL-1β blocking antibody led to reduced lung cancer incidence and mortality (Ridker et al., 2017a; Ridker et al., 2017b). Curiously, lung cancer is a type of cancer in which ChoKα is overexpressed, and is associated with high risk of recurrence (Huang et al., 2015; Ramirez

de Molina et al., 2007). ChoKα inhibitors may exert a similar effect and an added benefit due to a more direct effect on cancer cell proliferation.

Limitations of the Study

Our study links choline metabolism to the control of NLRP3 inflammasome dependent inflammation. The results implicate mitochondrial phospholipid remodeling as a key mechanism for preserving residual mitochondrial ATP synthase activity during the glycolytic switch that accompanies macrophage activation. Although we found that LPS altered mitochondrial lipid content by stimulation of choline uptake and phosphorylation, the exact mechanism through which phosphocholine synthesis affects mitochondrial ATP synthesis is unknown. In depth studies, investigating mitochondrial membrane plasticity and complex V structural organization after LPS-induced macrophage activation are needed. Our results indicate that CTL1 induction and elevated phosphocholine synthesis are important features of so-called macrophage priming, a process that enables macrophages to respond to a variety of NLRP3 activating challenges with IL-1β and IL-18 production and release. Although we find specific ChoKα inhibitors to be effective inhibitors of IL-1β and IL-18 dependent acute and chronic inflammation, full evaluation of the side effects of ChoKα inhibitors is needed before embarking on the use of such inhibitors in the clinic.

STAR METHODS

KEY RESOURCES TABLE

REAGENT or RESOURCE	SOURCE	IDENTIFIER
Antibodies		
IL-1β (WB:1/2000)	Cell Signaling	Cat#12426; N/A
phospho-Thr172 AMPK (WB:1/2500)	Cell Signaling	Cat#2535; ; N/A
VDAC	Cell Signaling	Cat#4161; RRID:AB_10557420
ATPIF1 (WB:1/2500)	Cell Signaling	Cat#8528; RRID:AB_10949890
CTL1 (WB:1/2500)	Assay Biotech	Cat#C21279; N/A
CTL1 (IF:1/100)	Proteintech	Cat#14687–1-AP; RRID:AB_10640573
AMPK (WB:1/5000)	Santa Cruz Biotechnology	Cat#25792; RRID:AB_2169546
DRP1 (WB:1/1000)	Santa Cruz Biotechnology	Cat#32898; RRID:AB_2093533
Tubulin (WB:1/10000)	Sigma-Aldrich	Cat#T9026; N/A
IKKβ (WB:1/2500)	Upstate	Cat#05–535; RRID:AB_2122161
Caspase-1 (WB:1/1000)	Adipogen	Cat#AG-20B-0042-C100; N/A
ASC (WB:1/5000)	Adipogen	Cat#AG-25b-0006-C100; N/A
NLRP3 (WB:1/5000)	Adipogen	Cat#AG-20B-0014-C100; N/A
p62 (WB:1/5000)	ProGen	Cat#GP62-C; RRID:AB_2687531
ChoKα (WB:1/2500; IF: 1/100)	Proteintech	Cat#13520–1-AP; RRID:AB_2079160
F4/80 (IF:1/100)	Invitrogen	Cat#MF48000; RRID:AB_1500089
Anti-ATP Synthase, beta chain, clone 4.3E8.D1 antibody (IF:1/100)	Millipore	Cat#MAB3494; RRID:AB_177597

REAGENT or RESOURCE	SOURCE	IDENTIFIER
Anti-rabbit IgG, HRP-linked Antibody (WB:1/5000)	Cell Signaling	Cat#7074; RRID:AB_2099233
Anti-mouse IgG, HRP-linked Antibody (WB:1/5000)	Cell Signaling	Cat#7076; RRID:AB_330924
Mouse IL-1beta /IL-1F2 Antibody	R&D Systems	Ca#MAB401; RRID:AB_2124620
Mouse IL-1beta /IL-1F2 Biotinylated Antibody	R&D Systems	Ca#BAF401; RRID: AB_356450
Anti-Mouse/Rat TNF alpha antibody	eBioscience	Cat#14–7423; RRID:AB_468492
Anti-Mouse/Rat TNF alpha Biotin antibody	eBioscience	Cat#13–7341; RRID:AB_466951
IL-6 Monoclonal Antibody (MP5–20F3)	eBioscience	Cat#14–7061-81; RRID:AB_468422
IL-6 Monoclonal Antibody (MP5–32C11), Biotin	eBioscience	Cat#13–7062-81; RRID:AB_466910
Anti-IL18 (mouse) m-Ab-Biotin	MBL	Cat#D048–6
Anti-IL18 (mouse) mAb	MBL	Cat#D047–3
Alexa Fluor® 647 Donkey Anti-Guinea Pig IgG (H+L)	Jackson Immuno Research Laboratories	Cat#706–606-148; RRID:AB_2340477
Donkey anti-rabbit IgG (H+L) secondary antibody, Alexa Fluor 488 (IF:1/350)	Invitrogen	Cat#A-21206; RRID:AB_2535792
Donkey anti-rabbit IgG (H+L) secondary antibody, Alexa Fluor 594 (IF:1/350)	Invitrogen	Cat#A-21207; RRID:AB_141637
Donkey anti-mouse IgG (H+L) secondary antibody, Alexa Fluor 488 (IF:1/350)	Invitrogen	Cat#A-21202; RRID:AB_141607
Donkey anti-mouse IgG (H+L) secondary antibody, Alexa Fluor 594 (IF:1/350)	Invitrogen	Cat#A-21203; RRID:AB_141633
Donkey anti-rat IgG (H+L) secondary antibody, Alexa Fluor 594 (IF:1/350)	Invitrogen	Cat#A-21209; RRID:AB_2535795
Bacterial and Virus Strains		
Specific lentiviral shRNA sequences	See Table 1	
Chemicals, Peptides, and Recombinant Proteins		
Recombinant Mouse IL-1β	R&D Systems	Cat#401-ML
Recombinant Mouse TNFα	eBioscience	Cat#14–8321
Recombinant Mouse IL-6	eBioscience	Cat#14–8061-62
Recombinant mouse IL-18	MBL	Cat#B002–5
Recombinant mouse GMCSF	R&D systems	Cat#415-ML
Ultrapure LPS, E. coli 0111:B4	Invivogen	Cat#tlrl-3pelps
Adenosine 5′-triphosphate disodium salt solution	Sigma-Aldrich	Cat#A6559
Nigericin	Invivogen	Cat#tlrl-..nig
Monosodium urate (MSU)	Enzo Life Science	Cat#ALX-400–047-M002
1,2-dioleoyl-3-trimethylammoniumpropane (DOTAP) liposomes	Encapsula NanoSciences (Zhong et al., 2016c)	N/A
Poly(dA:dT)	Invivogen	Cat#tlrl-patn
Oligomicyn	Millipore Sigma	Cat#O4876
Rotenone	Millipore Sigma	Cat#557368
A769662	Selleckchem	Cat#S2697
FURA-2, AM	Invitrogen	Cat#F-1221

REAGENT or RESOURCE	SOURCE	IDENTIFIER
PBFI, AM	Invitrogen	Cat#P1267MP
NP40 buffer	ThermoFisher Scientific	Cat#FNN0021
Complete™, Mini Protease Inhibitor Cocktail	Roche	Cat#11836153001
Phosphatase Inhibitor Cocktail 2	Sigma-Aldrich	Cat#P5726
Clarity Western ECL Substrate	Biorad	Cat#1705061
DAPI (4'6-Diamidino-2-Phenylindole, Dihydrochloride	Invitrogen	Cat#D1306
Tetramethylrhodamine, Methyl Ester, Perchlorate (TMRM)	Invitrogen	Cat#T668
MitoSOX™ Red mitochondrial superoxide indicator	Invitrogen	Cat#M36008
CellTiter-Glo Luminescent Assay	Promega	Cat#G924B
Bovine Serum Albumin	Gemini	Cat#700–100P
Triton X-100	Sigma-Aldrich	Cat#T8787
Normal horse serum	Vectorlabs	Cat#S-2000
Dimethyl Sulfoxide (DMSO)	Sigma-Aldrich	Cat#D2650–100
Protein Assay Dye reagent concentrate	Biorad	Cat#5000006
Polybrene	Sigma-Aldrich	Cat#TR-1003
FluorSave™	Millipore	Cat#345789
(Z)-4-hydroxytamoxifen	Sigma	Cat#H7604
Tamoxifen	MP Biomedicals	Cat#10378–016
RSM932A	Dr. Juan Carlos Lacal	N/A
MN58b	Dr. Juan Carlos Lacal	N/A
Sodium Chloride	Ricca Chemical company	Cat#7210–16
Trypsin-EDTA (0.25%)	Gibco	Cat# 25200056
Critical Commercial Assays		
Mitochondria isolation kit	ThermoFisher Scientific	Cat#89874
NAD^+/NADH cell-based assay kit	Cayman Chemical Company	Cat#600480
Complex V activity assay kit	Cayman Chemical Company	Cat#701000
Succinate colorimetric assay kit	Sigma Aldrich	Cat#MAK184–1KT
AllPrep DNA/RNA Mini kit	Qiagen	Cat#80204
Mouse IL-1β ELISA kit	R&D Systems	Cat#DY401
Lipofectamine™ 3000 Transfection Reagent	Invitrogen	Cat#L3000001
SuperScript™ VILO™ cDNA Synthesis Kit	Invitrogen	Cat#11754050
SsoAdvanced™ Universal SYBR Green Supermix	Biorad	Cat#172–5274
Experimental Models: Cell Lines		
HEK293T	ATCC	ATCC® CRL-3216™; RRID:CVCL_0063
L929	ATCC	ATCC® CCL-1™; RRID:CVCL_0462
Immortalized BMDM	Dr. Kate Fitzgerald	(N/A)
Experimental Models: Organisms/Strains		
C57BL/6	In house breeding	N/A
Ampka1$^{-/-}$	Dr. R. Liu-Bryan (Wang et al., 2016)	N/A

REAGENT or RESOURCE	SOURCE	IDENTIFIER
Il10rb$^{-/-}$	In house breeding	N/A
IKKβ$^{-/-}$	In house breeding	N/A
MWS *Nlrp3*^{A350VneoRCreT}	Dr. Hal M. Hoffman	N/A
FCAS *Nlrp3*^{L351PneoCreT}	Dr. Hal M. Hoffman	N/A
NOMID *Nlrp3*^{D301NneoCreT}	Dr. Hal M. Hoffman	N/A
Oligonucleotides		
Primers for mouse *Hprt1* *Forward:* CTGGTGAAAAGGACCTCTCG *Reverse:* TGAAGTACTCATTATAGTCAAGGGCA	Integrated DNA Technologies	N/A
Primers for mouse *ChKa* *Forward:* GCTGCAGTATACTAGATCTCCAGTTGT *Reverse:* ATCAGCTTCCGCCTTTCA	Integrated DNA Technologies	N/A
Primers for mouse *Chkb* *Forward:* GCAGAGGTTCAGAAGGGTGA *Reverse:* CCCCAGAAAAAGTGAGATGC	Integrated DNA Technologies	N/A
Primers for mouse *Slc44a1* *Forward:* TTTGCCCAAGCTACCAG *Reverse*: GAGCACAGCGATGGAAGAA	Integrated DNA Technologies	N/A
Primers for mouse *Slc44a2* *Forward:* CCTGGTGCTTGGCTATGG Reverse: CAAGGTCCAGGGAGA	Integrated DNA Technologies	N/A
Primers for mouse *Slc44a3* *Forward:* GGTCATTTTGGGATTGCTGT Reverse: ACTGAGGTCGTTGGTGTAGTCA	Integrated DNA Technologies	N/A
Primers for mouse *Slc44a4* *Forward:* ACTCTGTCCCCGTTTCCTTC Reverse: AAGTTGATGTTGGGGAGTGG	Integrated DNA Technologies	N/A
Primers for mouse *Slc44a5* *Forward:* ATCCAAGTGGCCATCATCC Reverse: GATTAACGCACTGGGAAGGT	Integrated DNA Technologies	N/A
Primers for mouse *Il1b* *Forward:* AGTTGACGGACCCCAAAAG *Reverse:* AGCTGGATGCTCTCATCAGG	Integrated DNA Technologies	N/A
Primers for mouse *Il6* *Forward:* CCAGGTAGCTATGGTACTCCA *Reverse*: GCTACCAAACTGGCTATAATC	Integrated DNA Technologies	N/A
Primers for mouse *Tnf* *Forward:* CCCTCACACTCAGATCATCTT *Reverse:* GCTACGACGTGGGCTACAG	Integrated DNA Technologies	N/A
Primers for mouse *Il10* *Forward:* CAGAGCCACATGCTCCTAGA *Reverse:* TGTCCAGCTGGTCCTTTGTT	Integrated DNA Technologies	N/A
Primers for mouse *Il10rb* *Froward:* TCTCTTCCACAGCACCTGAA *Reverse:* GAACACCTCGGCCTCCTC	Integrated DNA Technologies	N/A
Primers for mouse *Nos2* *Froward:* CTTTGCCACGGACGAGAC *Reverse:* TCATTGTACTCTGAGGGCTGAC	Integrated DNA Technologies	N/A
Primers for mouse *Cox1* *Forward:* GCCCCAGATATAGCATTCCC *Reverse:* GTTCATCCTGTTCCTGCTCC	Integrated DNA Technologies	N/A
Primers for mouse *D-loop* *Forward:* AATCTACCATCCTCCGTGAAACC *Reverse*: TCAGTTTAGCTACCCCCAAGTTTAA	Integrated DNA Technologies	N/A

REAGENT or RESOURCE	SOURCE	IDENTIFIER
Primers for mouse *18S* *Forward:* TAGAGGGACAAGTGGCGTTC *Reverse:* CGCTGAGCCAGTCAGTGT	Integrated DNA Technologies	N/A
Primers for mouse *Tert* *Forward:* CTAGCTCATGTGTCAAGACCCTCTT *Reverse:* GCCAGCACGTTTCTCTCGTT	Integrated DNA Technologies	N/A
Recombinant DNA		
VSV-G	(Zhong et al., 2016c)	N/A
pLV-CMVΔ8.9	(Zhong et al., 2016c)	N/A
shSlc44a1: 5'CCGGGCATCAGTGAATCGCCTTATTCTCGAGAATAAGGCGATTCACTGATGCTTTTTG3'	Sigma shRNA Mission library	N/A
shChka: 5'CCGGGTTACTTGACTACATTCCAAACTCGAGTTTGGAATGTAGTCAAGTAACTTTTTG3'	Sigma shRNA Mission library	N/A
shAtg7: 5'CCGGCCAGCTCTGAACTCAATAATACTCGAGTATTATTGAGTTCAGAGCTGGTTTTTG3'	Sigma shRNA Mission library	N/A
Software and Algorithms		
Prism 7.0	GraphPad Software	N/A
Other		
DMEM	Gibco	Cat#11995–065
DMEM	Gibco	Cat#11965–092
DMEM-F12	Gibco	Cat#11320033
CMRL1066	USBiological	Cat#C5900
CMRL1066 without choline	USBiological	Cat#C5900–07
Fetal Bovine Serum (FBS)	Gibco	Cat#10437–028 (lot.1913181)
Fetal Bovine Serum (FBS)	Corning	Cat#35–011-CV
Penicillin-streptomycin	Gibco	Cat#15140–122

CONTACT FOR REAGENT AND RESOURCE SHARING

Further information and requests for resources and reagents should be directed to and will be fulfilled according to institutional rules by the Lead Contact, Michael Karin (karinoffice@ucsd.edu).

EXPERIMENTAL MODEL AND SUBJECT DETAILS

Cell Lines and Primary Cultures

Macrophage culture and stimulation: Femurs and tibias from both female and male C57BL/6 mice, *Ampka1*$^{-/-}$ mice (kindly provided by Dr. R. Liu-Bryan), and *Il1Orb*$^{-/-}$ mice at 6–10 weeks of age were used to generate bone-marrow-derived macrophages (BMDM) as described (Hornung et al., 2008). Macrophages were cultured in DMEM supplemented with 10% FBS, 20% L929-cell conditioned medium, and 100 U/ml penicillin-streptomycin for 7–10 days. Bone marrow was isolated from MWS Nlrp3^{A350VneoRCreT}, FCAS Nlrp3^{L351PneoCreT}, and NOMID Nlrp3^{D301NneoCreT} conditional knock-in mice (Bonar et al., 2012; Brydges et al., 2009), and were allowed to differentiate over 7 days with addition of fresh mouse recombinant GMCSF every three days. (Z)-4-hydroxitamoxifen at 0.4 μg/ml

was added to cells 24 hr prior to treatment to induce the mutant *Nlrp3* allele. Immortalized mouse BMDM were obtained from Dr. Kate Fitzgerald and were grown in DMEM supplemented with 10% FBS and 100 U/ml penicillin-streptomycin. All cells were grown at 37 °C with 5% CO2. NLRP3 inflammasome activation was induced priming for 4 hr with ultrapure LPS (100 ng/ml) followed by treatment with the NLRP3 activators ATP (4 mM) and nigericin (10 μM) for 45 min, unless otherwise indicated, and monosodium urate (MSU) crystals (400 ĝ/ml) and 1,2-dioleoyl-3-trimethylammoniumpropane (DOTAP) liposomes (50 μg/ml) for 3 hr. In *Nlrp3* mutant macrophages IL-1β production was induced by LPS treatment for 16 hr at 37°C, whereas FCAS macrophages were incubated at 32°C without LPS addition. AIM2 inflammasome activation was induced by 4 hr LPS priming and transfection with lipofectamine 3000 and the AIM2 activator poly(dA:dT) (1 μg/ml) for 8 hr. For ChoKα inhibition, cells were treated with 5 RSM932A 8 hr (overnight) before LPS or 1 hr before LPS in the case of *Nlrp3* mutants. For choline deprivation experiments, the cells were cultured in CMRL1066 medium with or without choline for 2–3 hr before priming with LPS and kept during the experiment.

Microglia isolation: Primary microglia was isolated from wild type mice as previously described in (Saura et al., 2003). Microglia isolation and culture was performed by Dr Dorit Trudler at Dr Stuart Lipton laboratory at Scripps Research Institute. Briefly, mixed glial cultures were prepared from cerebral cortices of 1-day-old male C57BL/6 mice by mechanical and chemical dissociation and culture mixed glial cell in DMEM-F12 until confluency was achieved after 10–12 days. Then, microglial cultures were prepared by mild trypsinization (0.05 – 0.12 %) in the presence of 0.2–0.5 mM EDTA and 0.5–0.8 mM Ca2+ to detach an intact layer of astrocytes, leaving attached microglia. 15-Microglia were culture in DMEM-F12 supplemented with 10 % FBS for 15–21 days, then cells were detached and seed for experiment.

In Vivo Animal Studies—All mice used for experiments and primary culture were bred and maintained at University of California San Diego (UCSD) and were treated in accordance with guidelines of the Institutional Animal Care and Use Committee of UCSD. All mice are subjected to 12 hr light/dark cycles (light cycle from 6am to 6pm and dark cycle from 6pm to 6am) and are maintained at stable room temperature between 68–72 degrees Fahrenheit.

LPS-induced septic shock: Eight-to twelve-week-old male C57BL/6 mice were subjected to LPS-induced septic shock as described (Zhong et al., 2016c). Briefly, 50 mg/kg LPS was intraperitoneal (i.p.) injected, and when indicated, animals were pretreated with the ChoKα inhibitor MN58B 2.5 mg/kg or vehicle (Sodium Chloride) via i.p. injection daily, starting three days before LPS challenge. Mice were analyzed for survival and circulating cytokines (3 hr after LPS challenge). None of the animals was excluded from the analysis.

Synovium-like air pouch gout model: Subcutaneous air pouches were generated by repeated injection of sterile air in the back of eight-to twelve-week old female and males C57BL/6 mice to create an accessible space that develop developed a synovium-like membrane within 7 days as described (Wang et al., 2016). Afterwards, mice were treated

with MN58b i.p. (2.5 mg/kg) or vehicle, 24 hr before injecting 1 ml of MSU crystals (3 mg/ml) into the air pouch. Pouch tissue and fluids were harvested 8 hr later for analysis. None of the animals was excluded from the analysis.

Muckle Wells syndrome mice: Sixteen-to twenty-two-weeks-old males MWS $Nlrp3^{A350VneoRCreT}$ mutant mice were subjected to MN58b (2.5 mg/kg) or vehicle i.p. injection BID daily for 15 days. Tamoxifen (50 mg/kg) was administered daily via i.p. for 4 days after first MN58b (or vehicle) treatment, and once more on day 7 to maintain Cre expression. At the endpoint, blood, spleen and liver were collected for analysis. Complete blood counts were preformed using a ScilVet Animal Blood Counter (ABX Diagnostics). Livers were paraffin embedded and hematoxylin and eosine staining was performed to assess liver histology. None of the animals was excluded from the analysis and liver histology was blinded examined by two researchers.

METHOD DETAILS

shRNA lentiviral knockdown

Knockdown of *Slc44a1, ChoKα,* and *Atg7*was done by lentiviral transduction of immortalized BMDM as described (Zhong et al., 2016c). Sequences of target shRNAs used in this study were obtained from the MISSION shRNA Library (Sigma). Briefly, HEK293T cells were plated at 60% confluence in 6-well plates, and were transfected with 20 μl lipofectamine 3000 and 10 μg shRNA, 1 μg VSV-G and 5 μg pLV-CMVA8.9 plasmids, following manufacturer's instructions. Supernatants were collected 36 hr after transfection, filtered through 0.45 μm and added to iBMDM. To increase infection efficiency 8 ĝ/ml of polybrene was added. Virus containing medium was washed away after 6 hr and the cells were cultured with fresh medium. A second round of infection was done at 48 hr after the first round. Infected iBMDM were expanded and selected with puromycin.

Protein immunoblotting and ELISA

Mitochondria were isolated using Mitochondria Isolation kit. Whole cell lysates were prepared in NP40 buffer containing a protease inhibitor cocktail and a phosphatase inhibitor cocktail, and supernatants were analyzed by SDS-PAGE. Proteins were transferred into PVDF membranes, blocked in 5% BSA and 1X TBST for 1 hr, and incubated with indicated antibodies overnight. Secondary antibodies were added for 1 hr and detection was done using Clarity™ Western ECL Substrate (Biorad). Dilutions used for each antibodies are shown in the key resources table. Paired antibodies (capture and detection) and standard recombinant mouse IL-1β (R&D Systems), IL-18 (MBL), and TNF and IL-6 (eBioscience) were used to determine cytokine concentrations according to manufacturer's instructions.

RNA isolation and quantitative real-time PCR (QPCR)

RNA was extracted using AllPrep DNA/RNA Mini kit, and cDNA was synthesized using SuperScript™ VILO™ cDNA Synthesis Kit. mRNA expression was determined by QPCR in a CFX96 thermal cycler (Biorad) as described (Zhong et al., 2016c). Data are presented in arbitrary units and were calculated by 2ˆ(-delta delta CT) method. Primer sequences were

obtained from the NIH qPrimerDepot (http://mouseprimerdepot.nci.nih.gov) and provided by Integrated DNA technologies.

Immunofluorescence and confocal microscopy

Treated BMDM and pouch tissue were fixed in 4% paraformaldehyde, permeabilized in 0.01% Triton X-100, and blocked in 1X PBS supplemented with 2% BSA and 5% normal horse serum. Primary antibodies were incubated in blocking buffer at 4 °C overnight. Secondary Alexa antibodies from Life Technologies or Jackson Immuno Research Laboratories were added for 1 hr. Dilutions used for each antibody are shown in the key resources table. Nuclei were counterstained with DAPI. Samples were imaged through a Leica SP5 confocal microscope. Quantitation of p62 aggregates was measured in high magnification fields (HMF) and plotted as p62 aggregates per cell.

Choline and phosphocholine analysis by NMR

BMDM were treated with LPS for 4 hr and then were collected and processed for NMR analysis as described (Guma et al., 2015a; Tiziani et al., 2009). Polar metabolite isolation was performed using a modified Bligh-Dyer procedure (Wu et al., 2008). Extracts were dried using a CentriVap refrigerated vacuum concentrator (Labconco, Kansas City, MO, USA). Dried extracts were reconstituted in 100 mM phosphate buffer (pH 7.0) prepared in 10% H2O/90% D2O (Sigma) that contained 0.5 mM sodium 3-(trimethylsilyl)propionate-2,2,3,3,-d4 (TMSP) as the internal standard. One-dimensional ^{1}H NMR spectra were acquired on a Bruker Avance III 500 MHz with 1.7 mm TCI MicroCryoProbe system (Bruker BioSpin Corp., Billerica, MA) equipped with an autosampler at 300 K and processed as previously described (Lodi et al., 2017; Lu et al., 2017; Ludwig and Günther, 2011). Metabolite assignment and quantification were performed using the Chenomx 8.2 NMR Suite (Chenomx Inc., Edmonton, Alberta, Canada), the Birmingham Metabolite Library (Ludwig et al., 2012), and the Human Metabolome Database (Wishart et al., 2012).

Total phosphatidylcholine and mitochondrial lipids analysis by mass spectrometry

Total phosphatidylcholine (PC) analysis was measured in RSM932A-pretreated BMDM stimulated with LPS for 4 hr, while mitochondrial lipids were measured in mitochondria isolated from BMDM cultured in control or choline deficient medium and subjected to different treatments for 24 hrs. Samples were processed for UHPLC-MS/MS analysis and analysis was performed on a hybrid quadrupole-Orbitrap mass spectrometer (Q Exactive, Thermo Scientific, Bremen, Germany) coupled to an Accela 1250 UHPLC system equipped with a quaternary pump, vacuum degasser, and open autosampler with temperature controller (6°C; Fisher Scientific, San José, CA, USA). Chromatographic separation of metabolites was achieved by reverse phase (RP) analysis on a 150 mm × 2.1 mm Kinetex C18 (2.6 μm 100Å) column (Phenomenex Inc, Torrance, CA, USA) with the following conditions: solvent A, 60:40 water:acetonitrile with 10 mM ammonium formate and 0.1% formic acid; solvent B, 90:10 isopropanol:acetonitrile with 10 mM ammonium and 0.1% formic acid; separation gradient, initially 32% B, held for 2 minutes and then increased linearly from 32–99% B in 18 minutes, washing with 99% B for 5 minutes and column equilibration with 32% B for 10 minutes. The total run time was 35 minutes with a flow rate

of 0.25 mL/min and an injection volume of 5 μL. Ion detection was performed in full MS and MS/AIF modes with an electrospray (ESI) source simultaneously operating in fast negative/positive ion switching mode. The following acquisition settings were used for data collection in full MS mode: spray voltage, 4.0 kV; capillary temperature, 300°C; sheath gas, 51 (arbitrary units); auxiliary gas, 10 (arbitrary units); m/z range, 200–2000; data acquisition, centroid mode, microscans, 10; AGC target, 3e6; maximum injection time, 200 ms; mass resolution, 70,000 FWHM at m/z 200. The following parameters were modified as follows for full MS/AIF analysis: spray voltage, +3.5/−4.0 kV; capillary temperature, 250°C; sheath gas, 25 (arbitrary units); auxiliary gas, 15 (arbitrary units); higher-energy collisional dissociation (HCD), 10, 15, 20, 25, and 35 eV. The collision gas was nitrogen. Accuracy of analysis was ensured by calibrating the detector using commercial calibration solutions provided by the manufacturer. Mass tolerance was maintained at 5 ppm. The analytical platform was controlled by a computer operating the Xcalibur v. 2.2 SP1.48 software package (Thermo Scientific, San Jose, CA, USA). Raw files were processed using SIEVE 2.2.0 SP2 (Thermo Scientific) and the MATLAB programming environment (MathWorks, Natick, MA, USA). MS/MS fragmentation patterns were used to differentiate lipid classes. Features that did not achieve a relative standard deviation (RSD) of less than 0.25 in the quality control (QC) were excluded from analysis. Integrated peak intensities were normalized by the total spectral area and summed by class. The total intensity for each class was scaled to the vehicle control average for analysis.

Nitric oxide, calcium, and potassium flux measurements

BMDM were treated with LPS for 24 hr. NO production was measured in conditioned media as the concentration of nitrite by Griess reaction as described (Terkeltaub et al., 2011). Briefly, 50 μl of conditioned medium, or sodium nitrite standards were incubated with 50 μl of equal volumes of Griess reagents (Griess reagent A, 1 % sulfanilamide in 5 % phosphoric acid; and Griess reagent B, 0.1 % Napthylenediamine in H2O). Absorbance was measured at 490 nm.

Calcium and potassium fluxes were detected in BMDM cultured in control or choline-free medium treated with LPS and ATP, using FURA-2, AM (Invitrogen), and PBFI, AM (Invitrogen) respectively and flux was calculated according to manufacturer's instructions.

Mitochondrial function

Mitochondrial membrane potential (ψm) was measured using TMRM (#T668, Life Technologies) according to manufacturer's instructions. Briefly, RSM932A-pretreated BMDM and shCtrl and shChoKα iBMDM were primed with LPS for 4 hr. Cells were stained with 200 nM TMRM for 30 min at 37 °C, and then treated with CCCP (5 μM) for 5 min. After washing twice, fluorescence intensity was determined per manufacturer's instructions using a FilterMax F5 multimode plate reader (Molecular Devices), Mitochondrial reactive oxygen species (mtROS) was measured using MitoSOX (Invitrogen) as described (Zhong et al., 2016c). RSM932A-pretreated BMDM and shCtrl and shChoKα were primed with LPS for 4 hr and treated with nigericin and DOTAP for 30 min and 3 hr respectively. Cells were loaded with 4 μM MitoSOX for 20 min. After washing with PBS, fluorescence intensity was determined at 510/580 nm using a FilterMax F5 plate reader.

NAD^+/NADH ratio was measured using NAD^+/NADH Cell-Based Assay kit according to manufacturer's instructions (Cayman Chemical Company). Briefly, BMDM were aliquoted into 96-well plates treated with LPS for 24 hr. Cells were lysed and centrifuged. Supernatants and standards were incubated in reaction solution for 1.5 hr. Absorbance was measured at 450 nm using FilterMax F5 plate reader. Complex V ATP synthase activity was measured in mitochondria isolated from BMDM treated with LPS for 24 hr in the presence or absence of Oligomycin (10 μM), using Complex V Activity Assay kit (Cayman Chemical Company) according to manufacturer's instructions. Absorbance was measured at 340 nm at 30-second intervals for 30 min using a FilterMax F5 plate reader. Cellular ATP was measured after 24 hr LPS stimulation using CellTiter-Glo Luminescent Assay (Promega) as described (Ip et al., 2017). Succinate was measured in BMDM treated with indicated concentrations of LPS for 24 hr in either control or choline-deficient medium using the Succinate Colorimetric Assay kit (Sigma) according to manufacturer's instructions. Briefly, cells were homogenized in ice-cold succinate assay buffer, and after centrifugation, supernatants and succinate standards were incubated with reaction solution for 30 min at 37 °C. Absorbance was measured at 450 nm using FilterMax F5 plate reader.

Cellular fractionation and measurement of cytosolic mtDNA

BMDM were primed with LPS and stimulated with an NLRP3 inflammasome activator. Cellular fractionation was performed using Mitochondrial Isolation kit (ThermoScientific) according to manufacturer's instructions. Cytosolic mtDNA was analyzed as described (Nakahira et al., 2011). Briefly, DNA was isolated from 300 μl of the cytosolic fractions using All Prep DNA/RNA kit, and mitochondrial DNA encoding cytochrome c oxidase 1 and D-Loop were measured by QPCR with an equal volume of the DNA solution. Nuclear DNA encoding 18S ribosomal RNA and Tert was used for normalization. Primer sequences were obtained from the NIH qPrimerDepot (http://mouseprimerdepot.nci.nih.gov) and provided by Integrated DNA Technologies.

QUANTIFICATION AND STATISTICAL ANALYSIS

Data are shown as mean ± SD or mean ± SEM, as indicated. Statistical significance was determined using two-tailed student's t-test, and p values lower than 0.05 were considered statistically significant. Kaplan-Meier survival curves were analyzed by log rank test. All group numbers and detailed significant values are presented within the figure legends. Sample-sizes for mouse experiments were based on previous studies (Hoffman et al., 2010; Wang et al., 2016; Zhong et al., 2016c). GraphPad Prism was used for statistical analysis and graphing.

Supplementary Material

Refer to Web version on PubMed Central for supplementary material.

ACKNOWLEDGEMENTS

We thank eBioscience, Cell Signaling Technologies, Santa Cruz Technologies, Thermo Fisher, and Promega for gifts of reagents, Drs. Stuart Lipton and Dorit Trudler for providing primary mouse microglia cells; Christina Dooka, Lauren A Chang, and Lanchen Qu for technical help. Research was supported by NIH (R01AI43477 and

R37AI043477), NIEHS Superfund basic research program(P42ES010337), The Rotary Coins for Alzheimer's Research Trust Fund (CART Fund) awards to M.K., who is an American Cancer Research Society Professor and holds the Ben and Wanda Hildyard Chair for Mitochondrial and Metabolic Diseases; and LLS 7005–14 award to T.Kipps and M.K; VA Research Service Merit Review Awards (I01BX001660) and NIH/NIAMS (P50AR060772) to R.T.; and (1I01BX002234) and CymaBay Therapeutics grant to R.L-B.; NIH award to H.M.H. (R01DK113592), and NIH awards (R01AR073324 and R03AR068094) to M.G. E.S-L. was supported by Sara Borrell fellowship from ISCIII/MICINN. Z.Z. was supported by Cancer Research Institute Irvington Fellowship, Prevent Cancer Foundation Board of Directors Research Fund, and American Association for the Study of Liver Diseases Pinnacle Research Award. L.A. was supported by the International Cancer Research Fellowship (iCARE) and AIRC co-founded by the European Union. The support for the NMR facility was provided by the University of Texas Health Science Center at San Antonio and NIH/NCI (P30CA54174).

REFERENCES

References

Al-Saffar NM, Troy H, Ramirez de Molina A, Jackson LE, Madhu B, Griffiths JR, Leach MO, Workman P, Lacal JC, Judson IR, et al. (2006). Noninvasive magnetic resonance spectroscopic pharmacodynamic markers of the choline kinase inhibitor MN58b in human carcinoma models. Cancer Res 66, 427–434. [PubMed: 16397258]

Aoyama C, Liao H, and Ishidate K (2004). Structure and function of choline kinase isoforms in mammalian cells. Prog Lipid Res 43, 266–281. [PubMed: 15003397]

Ben-Neriah Y, and Karin M (2011). Inflammation meets cancer, with NF-kappaB as the matchmaker. Nat Immunol 12, 715–723. [PubMed: 21772280]

Bonar SL, Brydges SD, Mueller JL, McGeough MD, Pena C, Chen D, Grimston SK, Hickman-Brecks CL, Ravindran S, McAlinden A, et al. (2012). Constitutively activated NLRP3 inflammasome causes inflammation and abnormal skeletal development in mice. PLoS One 7, e35979. [PubMed: 22558291]

Brydges SD, Mueller JL, McGeough MD, Pena CA, Misaghi A, Gandhi C, Putnam CD, Boyle DL, Firestein GS, Horner AA, et al. (2009). Inflammasome-mediated disease animal models reveal roles for innate but not adaptive immunity. Immunity 30, 875–887. [PubMed: 19501000]

Busso N, and So A (2010). Mechanisms of inflammation in gout. Arthritis Res Ther 12, 206. [PubMed: 20441605]

Campanella M, Parker N, Tan CH, Hall AM, and Duchen MR (2009). IF(1): setting the pace of the F(1)F(o)-ATP synthase. Trends Biochem Sci 34, 343–350. [PubMed: 19559621]

Chen J, and Chen ZJ (2018). PtdIns4P on dispersed trans-Golgi network mediates NLRP3 inflammasome activation. Nature 564, 71–76. [PubMed: 30487600]

Chu AJ (1992). Bacterial lipopolysaccharide stimulates phospholipid synthesis and phosphatidylcholine breakdown in cultured human leukemia monocytic THP-1 cells. Int J Biochem 24, 317–323. [PubMed: 1733798]

Cordero MD, Williams MR, and Ryffel B (2018). AMP-Activated Protein Kinase Regulation of the NLRP3 Inflammasome during Aging. Trends Endocrinol Metab 29, 8–17. [PubMed: 29150317]

de la Roche M, Hamilton C, Mortensen R, Jeyaprakash AA, Ghosh S, and Anand PK (2018). Trafficking of cholesterol to the ER is required for NLRP3 inflammasome activation. J Cell Biol 217, 3560–3576. [PubMed: 30054450]

Egan DF, Shackelford DB, Mihaylova MM, Gelino S, Kohnz RA, Mair W, Vasquez DS, Joshi A, Gwinn DM, Taylor R, et al. (2011). Phosphorylation of ULK1 (hATG1) by AMP-activated protein kinase connects energy sensing to mitophagy. Science 331, 456–461. [PubMed: 21205641]

Elliott EI, and Sutterwala FS (2015). Initiation and perpetuation of NLRP3 inflammasome activation and assembly. Immunol Rev 265, 35–52. [PubMed: 25879282]

Glunde K, Bhujwalla ZM, and Ronen SM (2011). Choline metabolism in malignant transformation. Nat Rev Cancer 11, 835–848. [PubMed: 22089420]

Greten FR, Arkan MC, Bollrath J, Hsu LC, Goode J, Miething C, Goktuna SI, Neuenhahn M, Fierer J, Paxian S, et al. (2007). NF-kappaB is a negative regulator of IL-1beta secretion as revealed by genetic and pharmacological inhibition of IKKbeta. Cell 130, 918–931. [PubMed: 17803913]

Grove RI, Allegretto NJ, Kiener PA, and Warr GA (1990). Lipopolysaccharide (LPS) alters phosphatidylcholine metabolism in elicited peritoneal macrophages. J Leukoc Biol 48, 38–42. [PubMed: 2358751]

Guma M, Sanchez-Lopez E, Lodi A, Garcia-Carbonell R, Tiziani S, Karin M, Lacal JC, and Firestein GS (2015a). Choline kinase inhibition in rheumatoid arthritis. Ann Rheum Dis 74, 1399–1407. [PubMed: 25274633]

Guma M, Wang Y, Viollet B, and Liu-Bryan R (2015b). AMPK Activation by A-769662 Controls IL-6 Expression in Inflammatory Arthritis. PLoS One 10, e0140452. [PubMed: 26474486]

Guo WX, Pye QN, Williamson KS, Stewart CA, Hensley KL, Kotake Y, Floyd RA, and Broyles RH (2005). Mitochondrial dysfunction in choline deficiency-induced apoptosis in cultured rat hepatocytes. Free Radic Biol Med 39, 641–650. [PubMed: 16085182]

Hellberg S, Silvola JM, Kiugel M, Liljenback H, Metsala O, Viljanen T, Metso J, Jauhiainen M, Saukko P, Nuutila P, et al. (2016). Type 2 diabetes enhances arterial uptake of choline in atherosclerotic mice: an imaging study with positron emission tomography tracer (1)(8)F-fluoromethylcholine. Cardiovasc Diabetol 15, 26. [PubMed: 26852231]

Heneka MT, Kummer MP, Stutz A, Delekate A, Schwartz S, Vieira-Saecker A, Griep A, Axt D, Remus A, Tzeng TC, et al. (2013). NLRP3 is activated in Alzheimer's disease and contributes to pathology in APP/PS1 mice. Nature 493, 674–678. [PubMed: 23254930]

Hoffman HM, Scott P, Mueller JL, Misaghi A, Stevens S, Yancopoulos GD, Murphy A, Valenzuela DM, and Liu-Bryan R (2010). Role of the leucine-rich repeat domain of cryopyrin/NALP3 in monosodium urate crystal-induced inflammation in mice. Arthritis Rheum 62, 2170–2179. [PubMed: 20506351]

Hoffman HM, Wanderer AA, and Broide DH (2001). Familial cold autoinflammatory syndrome: phenotype and genotype of an autosomal dominant periodic fever. J Allergy Clin Immunol 108, 615–620. [PubMed: 11590390]

Hornung V, Bauernfeind F, Halle A, Samstad EO, Kono H, Rock KL, Fitzgerald KA, and Latz E (2008). Silica crystals and aluminum salts activate the NALP3 inflammasome through phagosomal destabilization. Nat Immunol 9, 847–856. [PubMed: 18604214]

Huang Z, Rui J, Li X, Meng X, and Liu Q (2015). Use of (1)(1)C-Choline positron emission tomography/computed tomography to investigate the mechanism of choline metabolism in lung cancer. Mol Med Rep 11, 3285–3290. [PubMed: 25591716]

Ip WKE, Hoshi N, Shouval DS, Snapper S, and Medzhitov R (2017). Antiinflammatory effect of IL-10 mediated by metabolic reprogramming of macrophages. Science 356, 513–519. [PubMed: 28473584]

James SJ, Cross DR, and Miller BJ (1992). Alterations in nucleotide pools in rats fed diets deficient in choline, methionine and/or folic acid. Carcinogenesis 13, 2471–2474. [PubMed: 1473260]

Lacal JC, and Campos JM (2015). Preclinical characterization of RSM-932A, a novel anticancer drug targeting the human choline kinase alpha, an enzyme involved in increased lipid metabolism of cancer cells. Mol Cancer Ther 14, 31–39. [PubMed: 25487918]

Lee GS, Subramanian N, Kim AI, Aksentijevich I, Goldbach-Mansky R, Sacks DB, Germain RN, Kastner DL, and Chae JJ (2012). The calcium-sensing receptor regulates the NLRP3 inflammasome through Ca2+ and cAMP. Nature 492, 123–127. [PubMed: 23143333]

Li B, and Webster TJ (2018). Bacteria antibiotic resistance: New challenges and opportunities for implant-associated orthopedic infections. J Orthop Res 36, 22–32. [PubMed: 28722231]

Lodi A, Saha A, Lu X, Wang B, Sentandreu E, Collins M, Kolonin MG, DiGiovanni J, and Tiziani S (2017). Combinatorial treatment with natural compounds in prostate cancer inhibits prostate tumor growth and leads to key modulations of cancer cell metabolism. NPJ precision oncology 1, 18. [PubMed: 29202102]

Lu X, Solmonson A, Lodi A, Nowinski SM, Sentandreu E, Riley CL, Mills EM, and Tiziani S (2017). The early metabolomic response of adipose tissue during acute cold exposure in mice. Scientific Reports 7, 3455. [PubMed: 28615704]

Ludwig C, Easton JM, Lodi A, Tiziani S, Manzoor SE, Southam AD, Byrne JJ, Bishop LM, He S, and Arvanitis TN (2012). Birmingham Metabolite Library: a publicly accessible database of 1-D 1H

and 2-D 1H J-resolved NMR spectra of authentic metabolite standards (BML-NMR). Metabolomics 8, 8–18.

Ludwig C, and Günther UL (2011). MetaboLab-advanced NMR data processing and analysis for metabolomics. BMC bioinformatics 12, 366. [PubMed: 21914187]

Martinon F, Mayor A, and Tschopp J (2009). The inflammasomes: guardians of the body. Annu Rev Immunol 27, 229–265. [PubMed: 19302040]

Martinon F, Petrilli V, Mayor A, Tardivel A, and Tschopp J (2006). Gout-associated uric acid crystals activate the NALP3 inflammasome. Nature 440, 237–241. [PubMed: 16407889]

Matter CM, Wyss MT, Meier P, Spath N, von Lukowicz T, Lohmann C, Weber B, Ramirez de Molina A, Lacal JC, Ametamey SM, et al. (2006). 18F-choline images murine atherosclerotic plaques ex vivo. Arterioscler Thromb Vasc Biol 26, 584–589. [PubMed: 16357314]

Mills EL, Kelly B, Logan A, Costa ASH, Varma M, Bryant CE, Tourlomousis P, Dabritz JHM, Gottlieb E, Latorre I, et al. (2016). Succinate Dehydrogenase Supports Metabolic Repurposing of Mitochondria to Drive Inflammatory Macrophages. Cell 167, 457–470 e413. [PubMed: 27667687]

Mills EL, and O'Neill LA (2016). Reprogramming mitochondrial metabolism in macrophages as an anti-inflammatory signal. Eur J Immunol 46, 13–21. [PubMed: 26643360]

Mishra BB, Rathinam VA, Martens GW, Martinot AJ, Kornfeld H, Fitzgerald KA, and Sassetti CM (2013). Nitric oxide controls the immunopathology of tuberculosis by inhibiting NLRP3 inflammasome-dependent processing of IL-1beta. Nat Immunol 14, 52–60. [PubMed: 23160153]

Munoz-Planillo R, Kuffa P, Martinez-Colon G, Smith BL, Rajendiran TM, and Nunez G (2013). K(+) efflux is the common trigger of NLRP3 inflammasome activation by bacterial toxins and particulate matter. Immunity 38, 1142–1153. [PubMed: 23809161]

Murakami T, Ockinger J, Yu J, Byles V, McColl A, Hofer AM, and Horng T (2012). Critical role for calcium mobilization in activation of the NLRP3 inflammasome. Proc Natl Acad Sci U S A 109, 11282–11287. [PubMed: 22733741]

Nakahira K, Haspel JA, Rathinam VA, Lee SJ, Dolinay T, Lam HC, Englert JA, Rabinovitch M, Cernadas M, Kim HP, et al. (2011). Autophagy proteins regulate innate immune responses by inhibiting the release of mitochondrial DNA mediated by the NALP3 inflammasome. Nat Immunol 12, 222–230. [PubMed: 21151103]

Narendra D, Tanaka A, Suen DF, and Youle RJ (2008). Parkin is recruited selectively to impaired mitochondria and promotes their autophagy. J Cell Biol 183, 795–803. [PubMed: 19029340]

Nomura J, So A, Tamura M, and Busso N (2015). Intracellular ATP Decrease Mediates NLRP3 Inflammasome Activation upon Nigericin and Crystal Stimulation. J Immunol 195, 5718–5724. [PubMed: 26546608]

O'Neill LA, and Hardie DG (2013). Metabolism of inflammation limited by AMPK and pseudo-starvation. Nature 493, 346–355. [PubMed: 23325217]

Ramirez de Molina A, Sarmentero-Estrada J, Belda-Iniesta C, Taron M, Ramirez de Molina V, Cejas P, Skrzypski M, Gallego-Ortega D, de Castro J, Casado E, et al. (2007). Expression of choline kinase alpha to predict outcome in patients with early-stage non-small-cell lung cancer: a retrospective study. Lancet Oncol 8, 889–897. [PubMed: 17851129]

Ridker PM, Everett BM, Thuren T, MacFadyen JG, Chang WH, Ballantyne C, Fonseca F, Nicolau J, Koenig W, Anker SD, et al. (2017a). Antiinflammatory Therapy with Canakinumab for Atherosclerotic Disease. N Engl J Med 377, 1119–1131. [PubMed: 28845751]

Ridker PM, MacFadyen JG, Thuren T, Everett BM, Libby P, Glynn RJ, and Group CT (2017b). Effect of interleukin-1beta inhibition with canakinumab on incident lung cancer in patients with atherosclerosis: exploratory results from a randomised, doubleblind, placebo-controlled trial. Lancet 390, 1833–1842. [PubMed: 28855077]

Roivainen A, Parkkola R, Yli-Kerttula T, Lehikoinen P, Viljanen T, Mottonen T, Nuutila P, and Minn H (2003). Use of positron emission tomography with methyl-11C-choline and 2–18F-fluoro-2-deoxy-D-glucose in comparison with magnetic resonance imaging for the assessment of inflammatory proliferation of synovium. Arthritis Rheum 48, 3077–3084. [PubMed: 14613269]

Rossi CR, Rossi CS, Sartorelli L, Siliprandi D, and Siliprandi N (1962). Protective action of phosphorylcholine on mitochondrial oxidative phosphorylation. Arch Biochem Biophys 99, 214–221. [PubMed: 13975170]

Saura J, Tusell JM, and Serratosa J (2003). High-yield isolation of murine microglia by mild trypsinization. Glia 44, 183–189. [PubMed: 14603460]

Schwarz T, Seidl C, Schiemann M, Senekowitsch-Schmidtke R, and Krause BJ (2016). Increased choline uptake in macrophages and prostate cancer cells does not allow for differentiation between benign and malignant prostate pathologies. Nucl Med Biol 43, 355–359. [PubMed: 27260776]

Seki M, Kawai Y, Ishii C, Yamanaka T, Odawara M, and Inazu M (2017). Functional analysis of choline transporters in rheumatoid arthritis synovial fibroblasts. Mod Rheumatol 27, 995–1003. [PubMed: 28121199]

Steinberg GR, and Kemp BE (2009). AMPK in Health and Disease. Physiol Rev 89, 1025–1078. [PubMed: 19584320]

Tannahill GM, Curtis AM, Adamik J, Palsson-McDermott EM, McGettrick AF, Goel G, Frezza C, Bernard NJ, Kelly B, Foley NH, et al. (2013). Succinate is an inflammatory signal that induces IL-1beta through HIF-1alpha. Nature 496, 238–242. [PubMed: 23535595]

Teodoro JS, Rolo AP, Duarte FV, Simoes AM, and Palmeira CM (2008). Differential alterations in mitochondrial function induced by a choline-deficient diet: understanding fatty liver disease progression. Mitochondrion 8, 367–376. [PubMed: 18765303]

Terkeltaub R, Yang B, Lotz M, and Liu-Bryan R (2011). Chondrocyte AMP-activated protein kinase activity suppresses matrix degradation responses to proinflammatory cytokines interleukin-1beta and tumor necrosis factor alpha. Arthritis Rheum 63, 1928–1937. [PubMed: 21400477]

Tian Y, Pate C, Andreolotti A, Wang L, Tuomanen E, Boyd K, Claro E, and Jackowski S (2008). Cytokine secretion requires phosphatidylcholine synthesis. J Cell Biol 181, 945–957. [PubMed: 18559668]

Tiziani S, Lodi A, Khanim FL, Viant MR, Bunce CM, and Gunther UL (2009). Metabolomic profiling of drug responses in acute myeloid leukaemia cell lines. PLoS One 4, e4251. [PubMed: 19158949]

Toyama EQ, Herzig S, Courchet J, Lewis TL Jr., Loson OC, Hellberg K, Young NP, Chen H, Polleux F, Chan DC, et al. (2016). Metabolism. AMP-activated protein kinase mediates mitochondrial fission in response to energy stress. Science 351, 275–281. [PubMed: 26816379]

Traiffort E, Ruat M, O'Regan S, and Meunier FM (2005). Molecular characterization of the family of choline transporter-like proteins and their splice variants. J Neurochem 92, 1116–1125. [PubMed: 15715662]

Trousil S, Kaliszczak M, Schug Z, Nguyen QD, Tomasi G, Favicchio R, Brickute D, Fortt R, Twyman FJ, Carroll L, et al. (2016). The novel choline kinase inhibitor ICL-CCIC-0019 reprograms cellular metabolism and inhibits cancer cell growth. Oncotarget 7, 37103–37120. [PubMed: 27206796]

Vallabhapurapu S, and Karin M (2009). Regulation and function of NF-kappaB transcription factors in the immune system. Annu Rev Immunol 27, 693–733. [PubMed: 19302050]

Wang Y, Viollet B, Terkeltaub R, and Liu-Bryan R (2016). AMP-activated protein kinase suppresses urate crystal-induced inflammation and transduces colchicine effects in macrophages. Ann Rheum Dis 75, 286–294. [PubMed: 25362043]

West AP, Brodsky IE, Rahner C, Woo DK, Erdjument-Bromage H, Tempst P, Walsh MC, Choi Y, Shadel GS, and Ghosh S (2011). TLR signalling augments macrophage bactericidal activity through mitochondrial ROS. Nature 472, 476–480. [PubMed: 21525932]

Wishart DS, Jewison T, Guo AC, Wilson M, Knox C, Liu Y, Djoumbou Y, Mandal R, Aziat F, and Dong E (2012). HMDB 3.0—the human metabolome database in 2013. Nucleic acids research 41, D801–D807. [PubMed: 23161693]

Wu H, Southam AD, Hines A, and Viant MR (2008). High-throughput tissue extraction protocol for NMR-and MS-based metabolomics. Analytical biochemistry 372, 204–212. [PubMed: 17963684]

Zhong Z, Liang S, Sanchez-Lopez E, He F, Shalapour S, Lin XJ, Wong J, Ding S, Seki E, Schnabl B, et al. (2018). New mitochondrial DNA synthesis enables NLRP3 inflammasome activation. Nature In Press.

Zhong Z, Sanchez-Lopez E, and Karin M (2016a). Autophagy, Inflammation, and Immunity: A Troika Governing Cancer and Its Treatment. Cell 166, 288–298. [PubMed: 27419869]

Zhong Z, Sanchez-Lopez E, and Karin M (2016b). Autophagy, NLRP3 inflammasome and auto-inflammatory/immune diseases. Clin Exp Rheumatol 34, 12–16. [PubMed: 27586797]

Zhong Z, Umemura A, Sanchez-Lopez E, Liang S, Shalapour S, Wong J, He F, Boassa D, Perkins G, Ali SR, et al. (2016c). NF-kappaB Restricts Inflammasome Activation via Elimination of Damaged Mitochondria. Cell 164, 896–910. [PubMed: 26919428]

Zhong Z, Zhai Y, Liang S, Mori Y, Han R, Sutterwala F, and Qiao L (2013). TRPM2 links oxidative stress to the NLRP3 inflammasome activation (P1268). J Immunol 190.

Zhou R, Yazdi AS, Menu P, and Tschopp J (2011). A role for mitochondria in NLRP3 inflammasome activation. Nature 469, 221–225. [PubMed: 21124315]

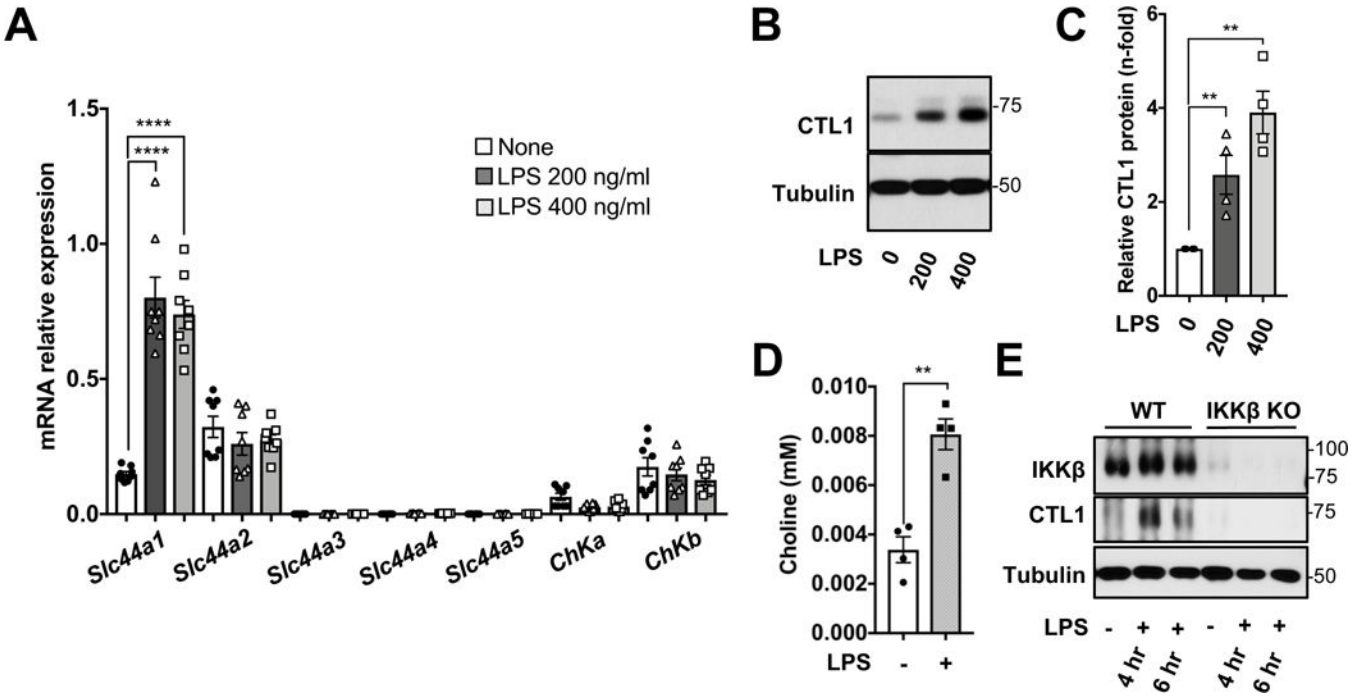

Figure 1. LPS stimulates choline uptake via NF-kB mediated CTL1 induction.

(A) QPCR analysis of mRNAs encoding choline transporters and kinases. Mean ± SEM (n = 8). **(B)** Immunoblot (IB) analysis of CTL1 4 hr after LPS addition. **(C)** Relative CTL1 protein expression in LPS stimulated BMDM. Mean ± SEM (n = 4). **(D)** Intracellular choline in BMDM before and 4 hr after LPS addition. Mean ± SEM (n = 4). **(E)** IB analysis of CTL1, IKKp and tubulin in WT or IKK$\beta^{-/-}$ LPS-stimulated BMDM. **p < 0.01; ***p < 0.005. See also Figure S1.

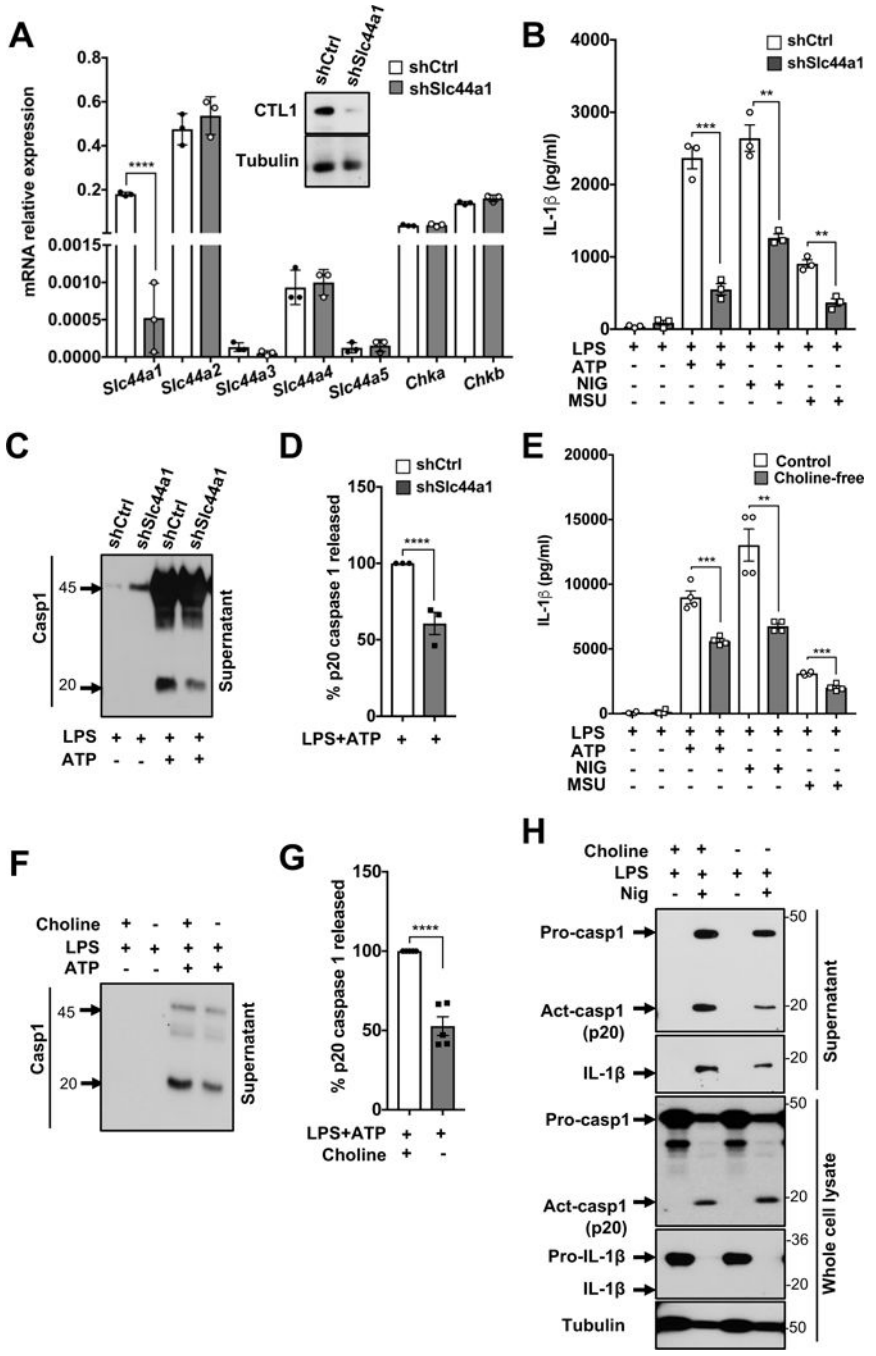

Figure 2. Choline deficiency or Slc44a1 knockdown reduce IL-1β production.

(A) QPCR analysis of mRNAs encoding choline transporters and kinases in shSlc44a1 and shControl (shCtrl) immortalized BMDM (iBMDM). Mean ± SD (n = 3). The inserts demonstrate the efficacies of *Slc44a1* silencing. **(B)** IL-1β release by shSlc44a1 and shCtrl iBMDM treated as indicated. Mean ± SD (n = 3). **(C)** IB analysis of caspase-1 in shSlc44a1 and shCtrl iBMDM treated as indicated. **(D)** Relative caspase 1 activation shown as % of p20 release to culture medium by iBMDM treated as in **(C)**. Mean ± SD (n = 3). **(E)** IL-1β release by BMDM cultured either in control or choline-deficient medium and treated as in

(B). Mean ± SEM (n = 4). **(F)** Caspase-1 in supernatants of LPS+ATP-treated BMDM cultured either in control or choline-deficient medium. **(G)** Relative caspase 1 activation shown as % of p20 release to culture medium by BMDM treated as in **(F)**. Mean ± SEM (n = 5). (H) IB analysis of caspase-1 and IL-1β in supernatants and lysates of LPS+nigericin-treated BMDM cultured in either control or choline-deficient medium. *p < 0.05; **p < 0.01; ***p < 0.005. See also Figure S2.

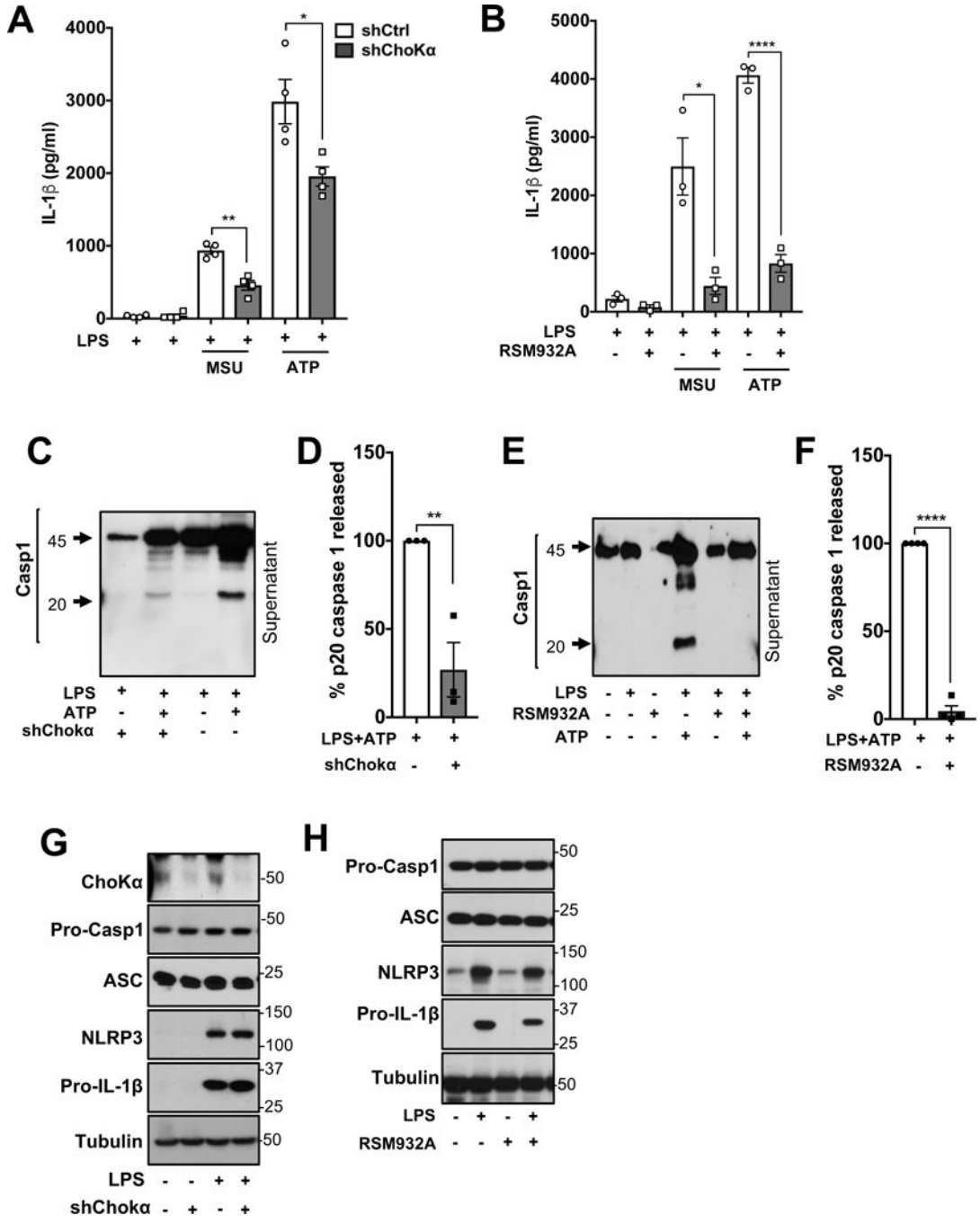

Figure 3. ChoKα knockdown and inhibition reduce IL-1β production.

(A) IL-1β release by shChoKα and shCtrl iBMDM treated as indicated. Mean ± SD (n = 3). **(B)** IL-1β release by LPS+ATP or LPS+MSU-stimulated BMDM pretreated with RSM932A. Mean ± SD. (n = 3). **(C)** Caspase-1 in supernatants of shChoKα and shCtrl iBMDM that were treated with LPS+ATP. (D) Relative caspase 1 activation shown as % of p20 release to culture medium by iBMDM cultured as in **(C)**. Mean ± SD (n = 3). **(E)** IB analysis of active caspase-1 in supernatants of BMDM pretreated with RSM932A and stimulated with LPS+ATP. (F) Relative caspase 1 activation in cells treated as above. Mean

± SEM (n = 4). **(G)** IB analysis of NLRP3 inflammasome subunits in shChoKα and shCtrl iBMDM or **(H)** BMDM pretreated with RSM932A as indicated. *p < 0.05; **p < 0.01.

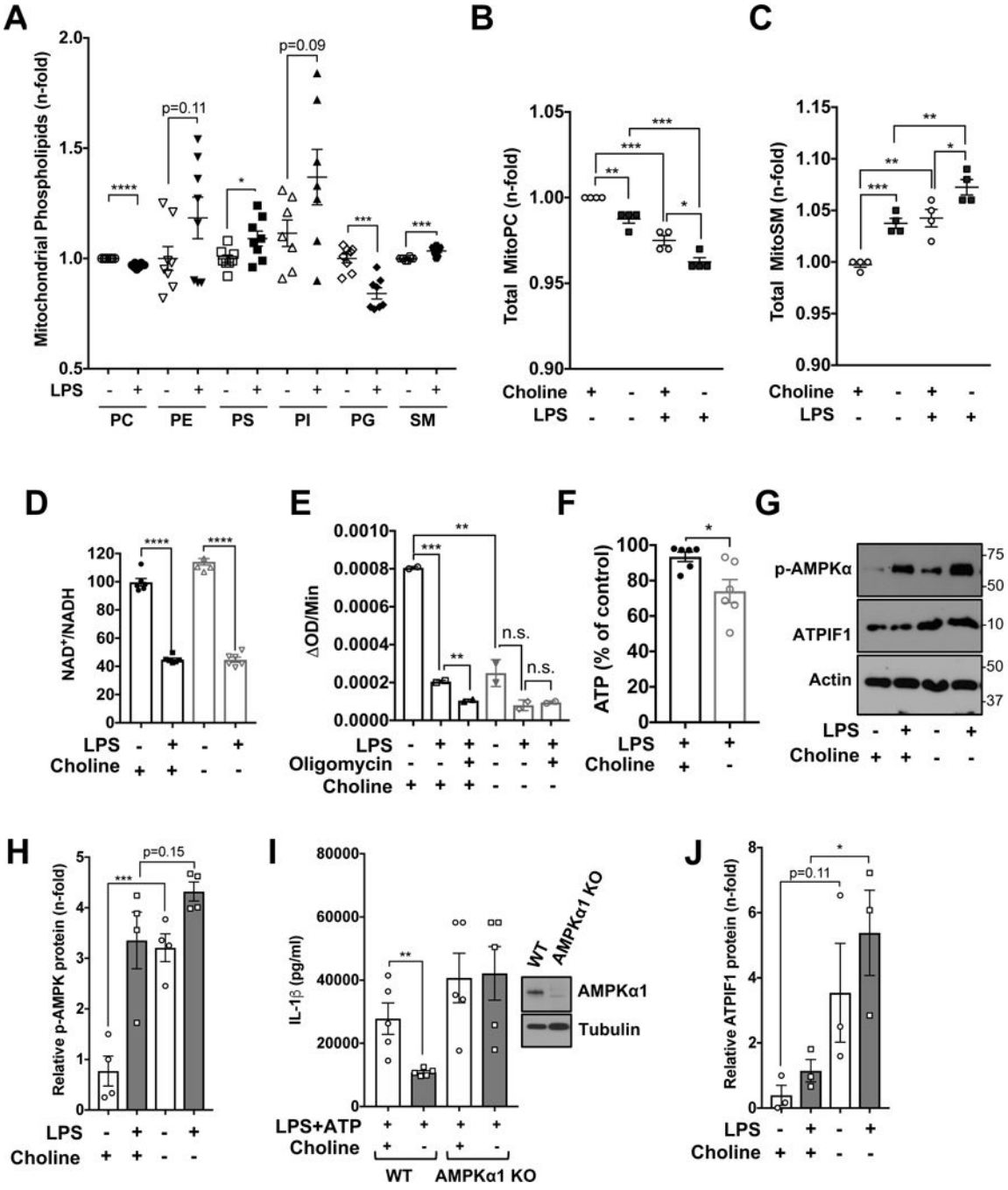

Figure 4. Choline deficiency alters mitochondrial lipids and depletes cellular ATP, resulting in AMPK activation and decreased IL-1β production.

(A) Relative amounts of mitochondrial phospholipids in BMDM before and 24 hr after LPS addition(n = 4). **(B)** Total mitochondrial phosphatidylcholine (mitoPC) and **(C)** sphingomyelin (mitoSM), in BMDM cultured in control or choline-deficient medium and incubated with or without LPS for 24 hr. (n = 4). **(D)** NAD^+/NADH ratio in BMDM cultured and treated as above. Mean ± SEM (n = 5). **(E)** ATP synthase activity in mitochondria isolated from BMDM that were cultured and treated as indicated. Mean ± SD (n = 2). **(F)**

Relative cellular ATP presented as % of control in BMDM cultured and treated as above. Mean ± SEM (n = 6). **(G)** IB analysis of p-AMPK, ATPIF1 in BMDM cultured and treated as above. **(H)** IB analysis of p-AMPK 24hr after LPS addition in the presence or absence of choline (n = 3). **(I)** IL-1β release by WT and *Ampkα1*$^{-/-}$ BMDM cultured in control or choline-deficient medium and stimulated with LPS+ATP. Mean ± SEM (n = 5). (J) IB analysis of ATPIF1 24 hr after LPS addition in the presence or absence of choline. (n = 3). *p < 0.05; **p < 0.01; ***p<0.05; ****p < 0.001. See also Figure S3.

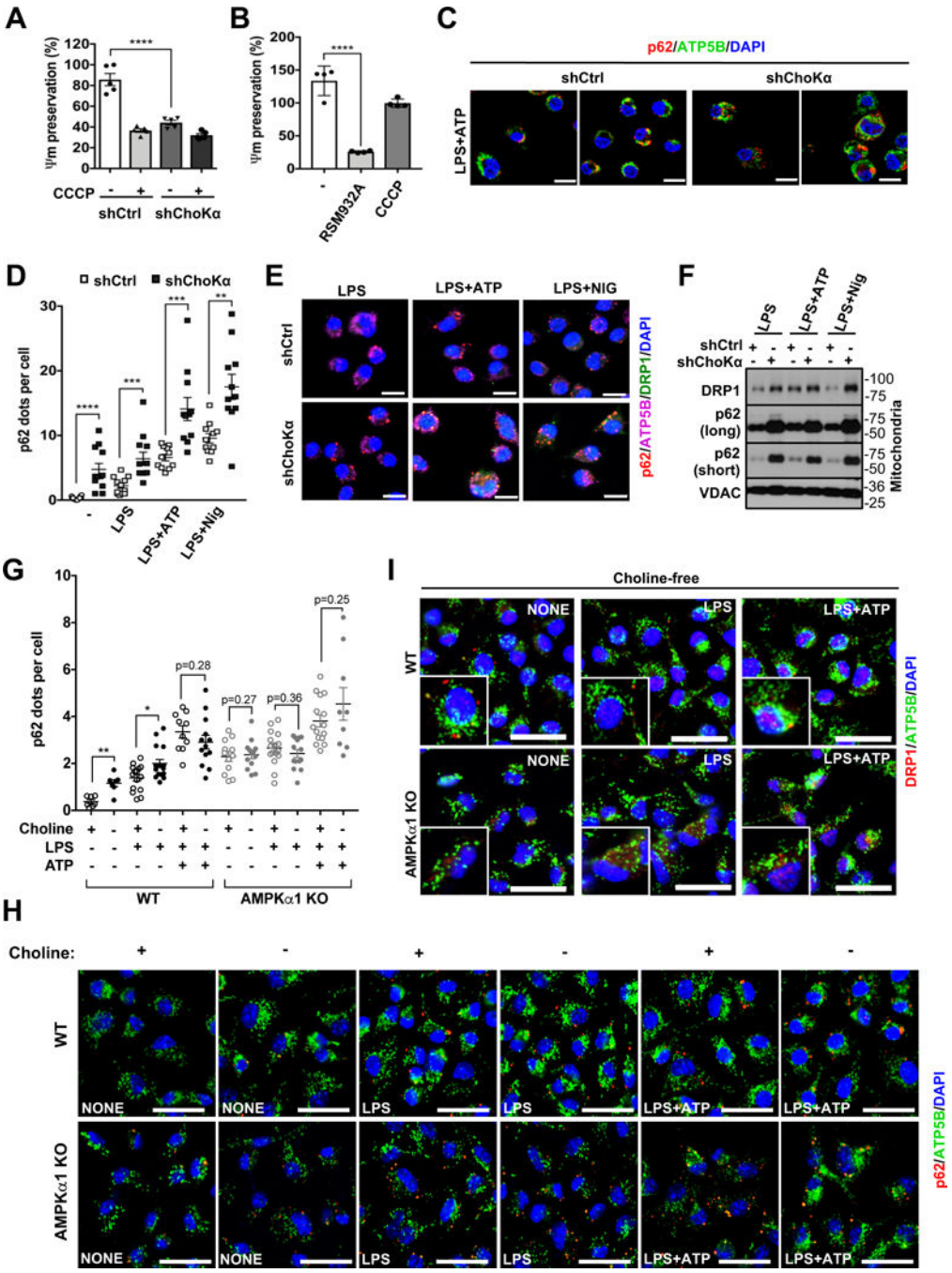

Figure 5. Impaired choline uptake and phosphorylation stimulate mitophagy and inhibit IL-1β production.

Mitochondrial membrane potential (Ψm) was measured in **(A)** shCtrl, shChoKα or **(B)** RSM932A-pretreated iBMDM by TMRM staining. Mean ± SEM (n = 5 and 4, respectively). **(C)** Immunofluorescence (IF) analysis of p62 recruitment to mitochondria stained by ATP5B antibody. Scale bar: 10 μm (images representative of three experiments). **(D)** Mitochondrial p62 aggregates. Mean ± SEM. (n = 10 HMF per treatment in two independent experiments). **(E)** IF analysis of p62 and DRP1 recruitment to mitochondria in LPS-primed and ATP or

nigericin-treated shChoKα and shCtrl iBMDM. Scale bar: 10 μm (images representative of three experiments). **(F)** IB analysis of p62, DRP1 and VDAC in mitochondria treated as indicated. **(G)** Mitochondrial p62 aggregates in WT and *Ampkα1*$^{-/-}$ BMDM treated as indicated. Mean ± SEM (n = 10–14 HMF per treatment in two independent experiments). **(H)** IF analysis of p62 recruitment to mitochondria. Scale bar: 20 μm (images representative of two experiments). **(I)** IF analysis of DRP1 and mitochondria stained by ATP5B antibody. Scale bar: 20μm (images representative of two experiments). *p < 0.05; **p<0.01; ***p < 0.005; ****p < 0.001. See also Figure S4.

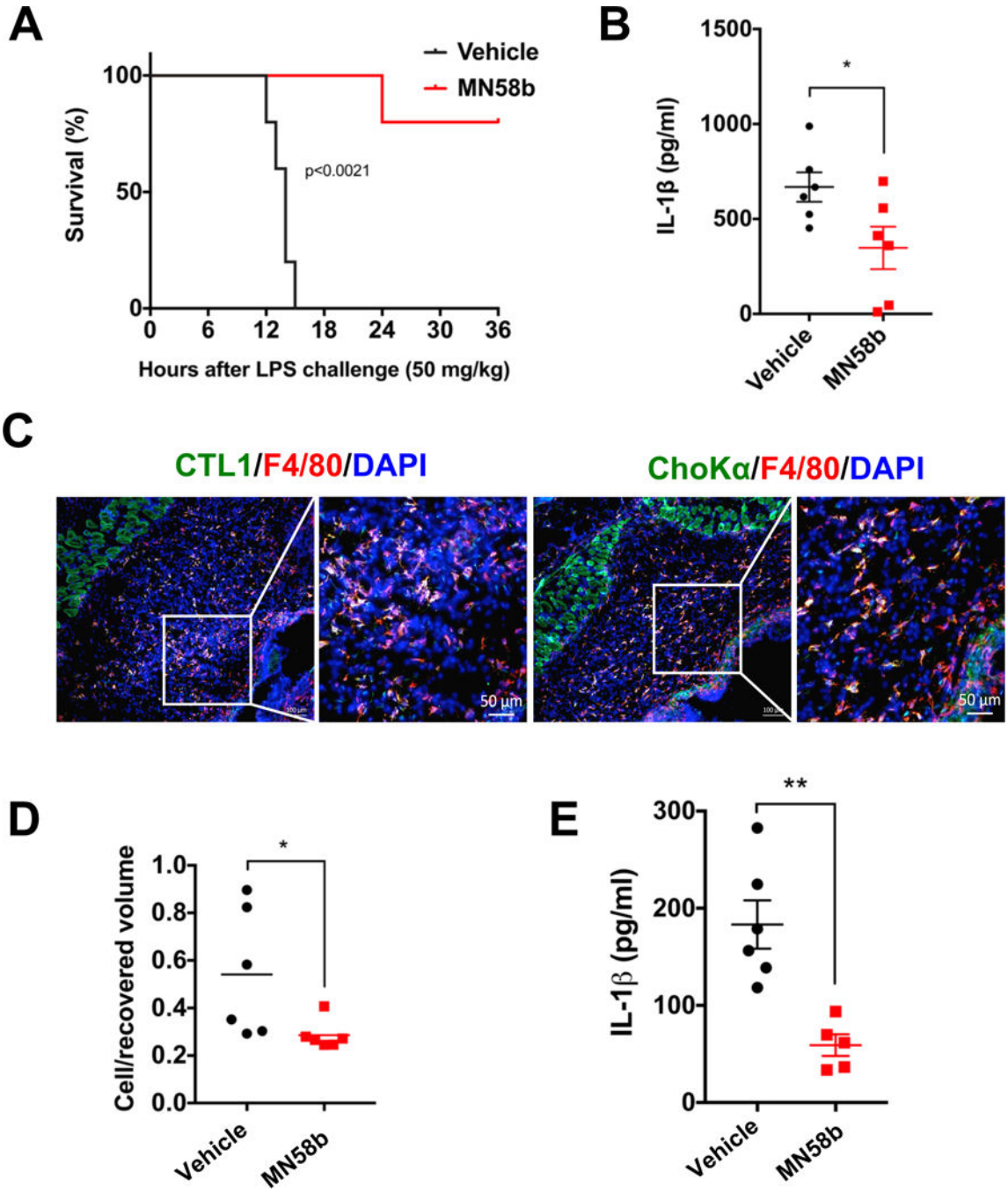

Figure 6. ChoKα inhibition reduces IL-1β production *in vivo*.

Mice were pretreated with ChoKα inhibitor MN58b or vehicle daily for 3 days before i.p. injection of 50 mg/kg LPS. **(A)** % survival was determined by Kaplan Meyer analysis and **(B)** circulating IL-1β by ELISA. Mean ± SEM (n = 6 animals per group). **(C-E)** Air pouches were created by s.c. injection of sterile air. Animals were treated with MN58b or vehicle 24 hr prior to injection of MSU crystals into the pouch. **(C)** IF analysis of cells stained with macrophage marker F4/80 and CTL1 or ChoKα antibodies in skin collected from air pouch after MSU crystals injection. Scale bar 50 μm. (D) Pouch cell counts. Mean ± SEM. (n = 6

mice per group). **(E)** IL-1β release into pouch cavity. Mean ± SEM (n = 6 animals per group). *p < 0.05; **p < 0.01. See also Figure S5.

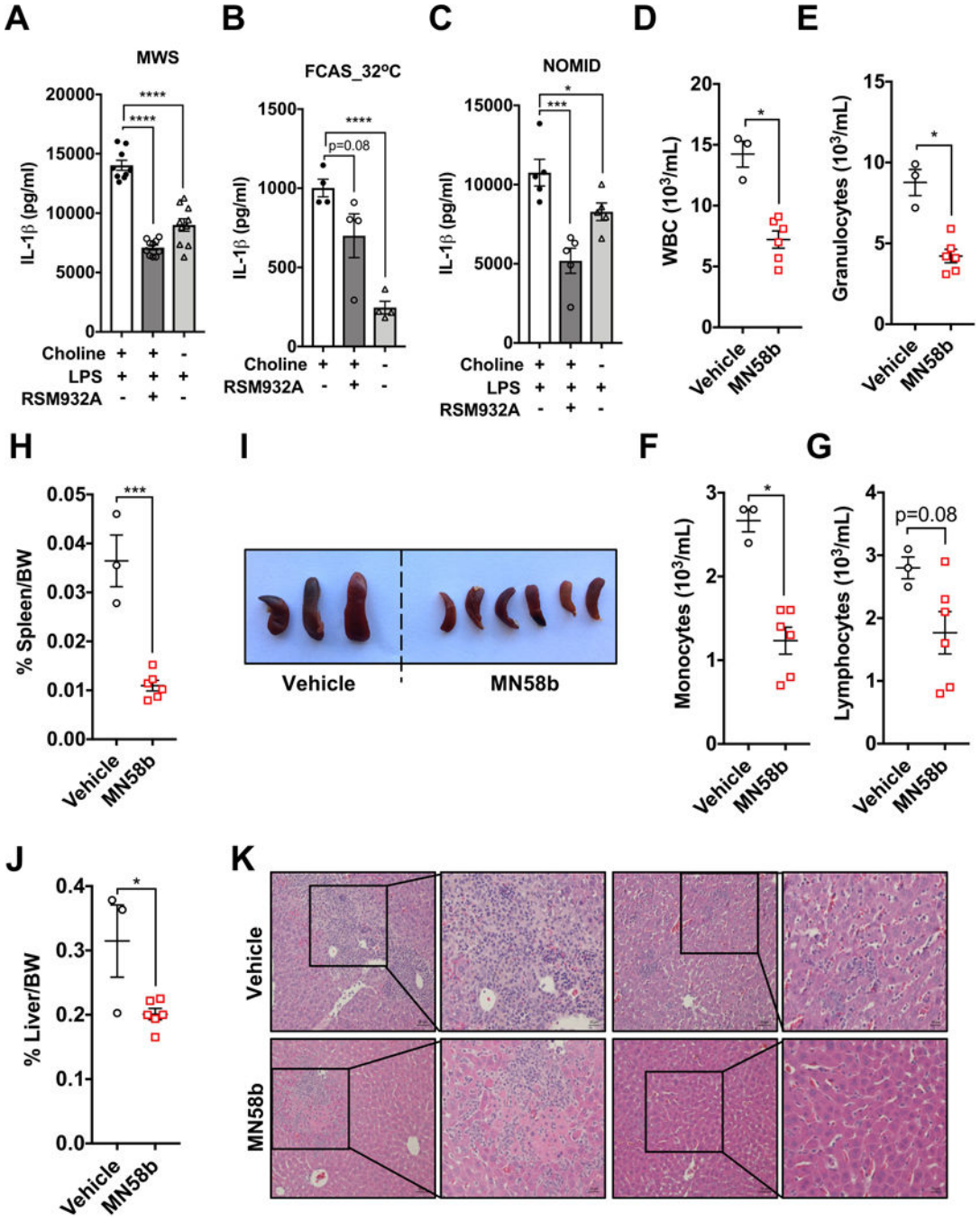

Figure 7. ChoKα inhibition reduces MWS pathology.

(A-C) IL-1β release by BMDM from mice containing MWS **(A)**, FCAS **(B)**, and NOMID **(C)** *Nirp3* mutations. The cells were cultured in control or choline-deficient medium or in the presence of ChoKα inhibitor RSM932A, and stimulated with LPS or in case of FCAS activated at 32°C. Mean ± SEM (n=10, MWS; n=4, FCAS; n=5, NOMID). **(D-K)** MWS $Nlrp3^{A350VneoRCreT}$ mice were treated with the ChoKα inhibitor MN58b or vehicle BID for 15 days. Circulating leukocytes **(D)**, granulocytes **(E)**, monocytes **(F)**, and lymphocytes **(G)**, were measured. **(H)** Spleen size as % spleen weight of body weight. **(I)** Image shows

spleens. **(J)** Liver size as % liver weight of body weight. **(K)** H&E staining of liver tissue from above mice. Mean ± SEM. (n = 3 vehicle and n = 6 MN58b treatment). *p < 0.05; ***p<0.005; ****p<0.001.